AFRL-RV-HA-TR-2007-1151

# Detection of Nuclear Explosions Using Infrasound Techniques

D. R. Christie
B. L. N. Kennett

Research School of Earth Sciences
The Australian National University
Mills Road
Canberra, A.C.T. 0200
Australia

Final Report

1 December 2007



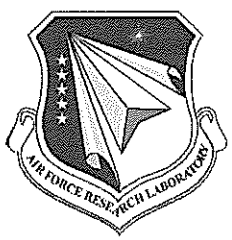


AIR FORCE RESEARCH LABORATORY
Space Vehicles Directorate
29 Randolph Road
AIR FORCE MATERIEL COMMAND
Hanscom AFB, MA 01731-3010

## NOTICE AND SIGNATURE PAGE

Using Government drawings, specifications, or other data included in this document for any purpose other than Government procurement does not in any way obligate the U.S. Government. The fact that the Government formulated or supplied the drawings, specifications, or other data does not license the holder or any other person or corporation; or convey any rights or permission to manufacture, use, or sell any patented invention that may relate to them.

This report was cleared for public release and is available to the general public, including foreign nationals. Qualified requestors may obtain additional copies from the Defense Technical Information Center (DTIC) (http://www.dtic.mil). All others should apply to the National Technical Information Service.

AFRL-RV-HA-TR-2007-1151 HAS BEEN REVIEWED AND IS APPROVED FOR PUBLICATION IN ACCORDANCE WITH ASSIGNED DISTRIBUTION STATEMENT.

| //Signature// | //Signature// |
|---|---|
| ROBERT RAISTRICK<br>Contract Manager | PAUL TRACY, Acting Chief<br>Battlespace Surveillance Innovation Center |

This report is published in the interest of scientific and technical information exchange, and its publication does not constitute the Government's approval or disapproval of its ideas or findings.

# REPORT DOCUMENTATION PAGE [example]

*Form Approved*
*OMB No. 0704-0188*



| **1. REPORT DATE** *(DD-MM-YYYY)* | **2. REPORT TYPE** | **3. DATES COVERED** *(From - To)* |
|---|---|---|
| 01-12-2007 | Final Report | 14-09-2004 to 14-09-2007 |

**4. TITLE AND SUBTITLE**
Detection of Nuclear Explosions Using Infrasound Techniques

**5a. CONTRACT NUMBER**
FA8718-04-C-0032

**5b. GRANT NUMBER**

**5c. PROGRAM ELEMENT NUMBER**
62601F

**6. AUTHOR(S)**
Dr. D.R. Christie and Professor B.L.N. Kennett

**5d. PROJECT NUMBER**
1010

**5e. TASK NUMBER**
SM

**5f. WORK UNIT NUMBER**
A1

**7. PERFORMING ORGANIZATION NAME(S) AND ADDRESS(ES)**
Research School of Earth Sciences
The Australian National University
Canberra, A.C.T. 0200
Australia

**8. PERFORMING ORGANIZATION REPORT NUMBER**

**9. SPONSORING / MONITORING AGENCY NAME(S) AND ADDRESS(ES)**

Air Force Research Laboratory
29 Randolph Rd.
Hanscom AFB, MA 01731-3010

**10. SPONSOR/MONITOR'S ACRONYM(S)**
AFRL/RVBYE

**11. SPONSOR/MONITOR'S REPORT NUMBER(S)**
AFRL-RV-HA-TR-2007-1151

**12. DISTRIBUTION / AVAILABILITY STATEMENT**

Approved for Public Release; Distribution Unlimited.

**13. SUPPLEMENTARY NOTES**

**14. ABSTRACT**
The performance of typical IMS infrasound monitoring stations has been examined in detail in order to evaluate the detection capability of the global network for regional and distant nuclear explosions. Three significant problems have been identified: a) problems with the loss of higher frequency signal components in the primary monitoring passband, b) detection problems associated with a low degree of signal coherence between array elements and c) problems with high levels of wind-generated background noise. Loss of higher frequency signal components normally occurs when signal propagation is restricted to a thermospheric waveguide. This problem can often be resolved by ensuring that routine processing algorithms include a long-period passband. Coherence studies show that detection capability for regional and distant explosions may be limited by the small degree of signal correlation between array elements. This problem can be resolved by modifications to the array configuration. Wind-generated background noise is a potentially serious problem at most infrasound monitoring stations. We have developed a new wind-noise-reducing system that effectively eliminates wind-generated noise in the monitoring passband. This system is based on the use of a closed screened enclosure that mechanically degrades turbulent eddies in the atmospheric boundary layer. This system can be used as an effective, stand-alone wind-noise-reducing system that does not require the use of a pipe array.

**15. SUBJECT TERMS**
Infrasonic Waves, Explosion Monitoring, Signal Correlation, Noise Reduction

| **16. SECURITY CLASSIFICATION OF:** | | | **17. LIMITATION OF ABSTRACT** | **18. NUMBER OF PAGES** | **19a. NAME OF RESPONSIBLE PERSON** |
|---|---|---|---|---|---|
| **a. REPORT** | **b. ABSTRACT** | **c. THIS PAGE** | | | Robert Raistrick |
| UNCLASSIFIED | UNCLASSIFIED | UNCLASSIFIED | SAR | 75 | **19b. TELEPHONE NUMBER** *(include area code)* 781-377-3726 |

# Table of Contents

# Figures

# Tables

## Acknowledgments

We would like to thank Dr. David Brown for many valuable discussions and for providing the detection algorithm that is used in this work. We would also like to thank Dr. Chris Tarlowski for assistance with data processing and fieldwork.

# 1. SUMMARY

The principal goals of this investigation are to identify problems with the detection of explosion-generated infrasonic signals at stations in the global infrasound monitoring network and to develop new techniques that will enhance the use of infrasound for the detection, location and discrimination of atmospheric nuclear explosions. This work is focused primarily on a detailed investigation of three important problems. The first part is concerned with problems associated with the loss of higher frequency signal components in the primary monitoring passband (0.4 to 1.2 Hz) when wave propagation is restricted to a thermospheric waveguide. The second part is focused on the limitations imposed on array detection of explosion-generated infrasound by the loss of signal correlation between elements in large sparse arrays. Finally, the third part of this investigation encompasses the long-standing problem in the field of infrasound monitoring of unacceptably high levels of background noise caused by wind-generated turbulence. This study is also concerned with the identification and classification of the fundamental physical processes that result in background noise at all frequencies at infrasound monitoring stations. The results of this study are based on a thorough analysis of a large infrasound database comprising six years of archived data from IS07 Warramunga in northern Australia, three years of archived data from IS05 Hobart in Tasmania, a one-year archive of data from IS04 Shannon in southwest Australia, shorter periods of selected data from other IMS infrasound stations and data collected during a number of field experiments in Australia using a portable infrasonic array.

The complete loss of higher frequency signal components from distant explosions in the primary monitoring passband is a potentially serious problem. This problem usually occurs when wave propagation is restricted to a thermospheric waveguide. There has been a tendency in recent years to restrict the routine analysis of data from the global infrasound network to frequencies that lie above the microbarom passband. We have found, however, that thermospheric signals from distant explosions can often be detected in a long-period passband centered at frequencies below the microbarom passband. In some cases, we have detected both high frequency stratospheric and low frequency thermospheric signals from distant explosions. The detection of these two phases can be used to improve location estimates and to help in the identification process. It is clear that both high frequency and low frequency passbands should be used in routine detection algorithms.

We have found good agreement between observations and the predictions of the Mack and Flinn (1971) coherence model and have applied this model to arbitrary array configurations to determine the predicted azimuthal distribution of the array-averaged correlation coefficient. The predicted array-averaged correlation coefficient provides a unique characteristic of the array configuration, which can be used as a measure of array performance. An examination of the azimuthal distribution of the predicted array-averaged correlation coefficient for IMS arrays with a small number of widely separated array elements shows that that loss of signal correlation between array elements in these arrays can seriously limit the reliable detection of infrasound generated by distant

explosions in the primary monitoring passband. We have also applied this analysis to typical IMS infrasound arrays with a large number of array elements and have found that signal correlation problems usually result in some loss of detection capability. Furthermore, in some cases, the analysis shows that the sensitivity of an array configuration may exhibit a significant azimuthal dependence. The design of infrasound monitoring arrays needs to be optimized to eliminate both spatial aliasing problems and signal coherence problems. We have developed 8-element and 9-element optimized infrasonic arrays designs, which are suitable for use in the global monitoring network.

Considerable progress has been made on the development of a noise-reducing system that can strongly attenuate, and in most cases, effectively eliminate wind-generated background noise in the monitoring passband at infrasound monitoring stations. Wind-generated noise is a serious problem, especially during the daytime, at many infrasound stations. Work on wind-noise reduction in the past has been primarily concerned with the development of improved wind-noise-reducing pipe-array systems. It is clear that further refinements to these pipe array systems will not lead to a significant improvement in wind-noise-reducing capability since the size of these arrays and the number of inlet ports have reached practical limitations. We have therefore developed a new type of wind-noise-reducing system which mechanically attenuates and degrades turbulent eddies that generate noise in the primary monitoring passband. The design and performance of a wide variety of these turbulence-reducing systems is given in this report along with recommendations for the use of these systems. The latest version of this system has proven to be very effective. Indeed, tests have shown that this system almost completely eliminates wind noise in the primary monitoring passband under typical daytime wind conditions at an unsheltered semi-desert site. In addition, we have found, in some circumstances, that these turbulence-reducing enclosures may be used with only a single inlet port as effective stand-alone wind-noise reducing systems that do not require a pipe array.

## 2. INTRODUCTION

The primary objectives of this research project are:

- To identify problems with the detection, location and discrimination of atmospheric nuclear explosions and
- To develop techniques using infrasound technology that will improve detection, location and discrimination capability for nuclear explosions in the atmosphere.

This project is concerned with the detection capability of the global IMS infrasound network for small nuclear explosions. The establishment of the IMS infrasound network is proceeding rapidly (see Figure 1). The average separation between nearest neighboring IMS infrasound stations is 1920 km in the Northern Hemisphere and 2027 km in the Southern Hemisphere. It is clear, however, that good detection capability is required for small nuclear explosions located at distances of more than 2000 km. For example, the distance between stations on opposite sides of the vast open ocean areas in the Southern Hemisphere may exceed 7000 km. Stations that monitor the open ocean areas in the Southern Hemisphere therefore need to have good detection capability for nuclear explosions that occur at distances of at least 4000 km.

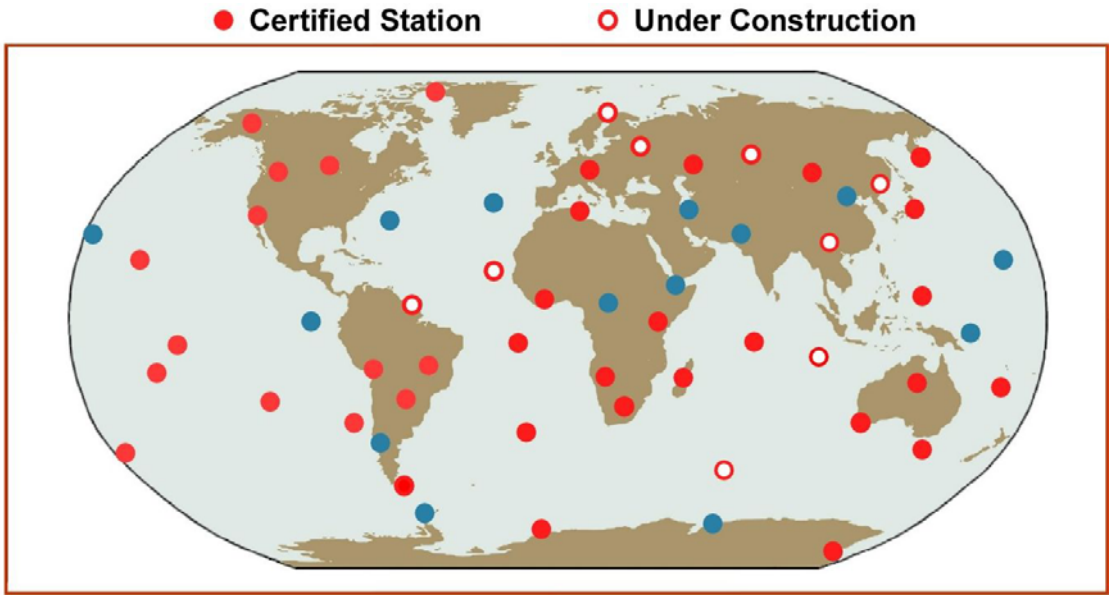


Figure 1. Current status of the 60-station IMS infrasound network.

At the present time, the global infrasound network is limited to two-station detection for nuclear explosions with a yield of 1-kiloton or more. Global three-station detection capability for a 1-kiloton explosion is desirable since this would greatly enhance the reliability of the network, lower the global detection threshold and significantly reduce location errors.

A brief description of the type and location of the sources and infrasound recording stations used in this project is given in Section 3.

Much of the research in this project is based on a survey of signal detection capability and background noise characteristics of certified Australian IMS monitoring stations. This survey has highlighted three important problems that may limit the performance of stations in the global monitoring network:

a) Distant explosions may be detectable only as longer period signals (Christie et al., 2005a) when wave propagation is restricted to a thermospheric waveguide. Problems associated with the decay of higher frequency signal components at a given station will depend on the location and distance to the source and the seasonal waveguide characteristics between the source and the monitoring array. The detection of thermospheric signals from distant explosions is discussed in Section 4.1.

b) The optimum monitoring passband (Christie et al. 2005b; 2006) for stratospheric arrivals from regional and distant explosions is limited to a frequency range extending from about 0.4 Hz to slightly above 1.0 Hz. The lower frequency limit depends on the intensity of microbarom infrasonic signals and the high frequency

limit is determined by both spatial aliasing of higher frequency signals and problems with signal coherence between array elements. The detection of higher frequency signals depends critically on the design of the array configuration. Spatial aliasing problems can be eliminated by using an eight- or nine-element array configured in the form of a logarithmic spiral or in the form of a larger aperture pentagon array with a smaller aperture triangular sub-array (or centered triangle sub-array) located at the center of the main array. Signal coherence between array elements at higher frequencies also depends on the array configuration. Results obtained to date have shown that detection capability for regional and distant explosions at existing monitoring stations with a small number of array elements and a large aperture will be marginal due to the low degree of signal coherence between array elements. The study of signal coherence is proving to be a fairly complex subject. The goal of this part of the project is to provide an accurate signal coherence model that can be used to optimize the array design at infrasound monitoring stations. Problems with signal coherence and the development of a method that can be used in the design of an optimal infrasound array are described in Section 4.2. This method is used to determine optimal array configurations that are suitable for use in the global infrasound monitoring network.

c) Wind-generated background noise has long been recognized as the most important technical issue in the field of infrasonic monitoring. More than half of the stations in the global monitoring network are subject at times to unacceptably high levels of wind-generated background noise. It is clear that the development of a system that will significantly reduce and possibly eliminate wind-generated noise at infrasound monitoring stations would greatly enhance the performance of the IMS infrasound monitoring network and would lower the global monitoring threshold. The use of an effective and reliable wind-noise suppressing system at IMS infrasound stations would probably result in global three-station detection capability for 1-kiloton nuclear explosions. The development of a new and very effective wind-noise-reducing system is described in Section 4.3. Results from this new noise-reducing system suggest that the use of this system, either as a stand-alone system, or in conjunction with existing pipe arrays, can nearly eliminate wind-noise in the primary monitoring passband.

This investigation has led to a number of conclusions and recommendations regarding the design of infrasound monitoring stations and the processing of infrasonic data. The conclusions are discussed in Section 5 and a list of recommendations is given in Section 6.

# 3. METHODS AND PROCEDURES

## 3.1. Sources of Data

The research in this project is based primarily on a detailed investigation of explosion-generated infrasonic signals recorded at certified Australian IMS monitoring stations and at a number of temporary stations established for short periods of time at carefully selected locations on the Australian continent using a portable infrasonic array.

Five IMS infrasound monitoring stations are located on Australian territory. Three of these stations, IS04 Shannon, IS05 Hobart and IS07 Warramunga, have been in operation for some time. Work on the construction of a 4th Australian station, IS06 Cocos Islands, is underway and it is expected that the last Australian station in the IMS network, IS03 Davis Base in Antarctica, will be established in early 2009. The locations of the three certified infrasound stations on the Australian mainland, the location of the most important open-cut mines, and the sites of the temporary infrasonic arrays are shown in Figure 2. The locations of the New South Wales bolide on 5 December 2004 and the Manam Volcano explosion on 27 Jan 2005 are also shown on this map, along with the location of a 0.027 kT chemical explosion at the Woomera Test Range. Only the most significant open-cut mines and mining areas are shown in Figure 2. A large number of smaller mines have been omitted since explosions at these mines tend to be of lower yield and signals from these explosions are usually detected only at local or near-regional distances. The data set also includes signals from a number of minor volcanic eruptions located in the active volcanic arc to the northeast, north and northwest of the Australian continent, signals generated by large earthquakes, and a few other bolide explosions. The locations of these events have also been omitted from the map in Figure 2.

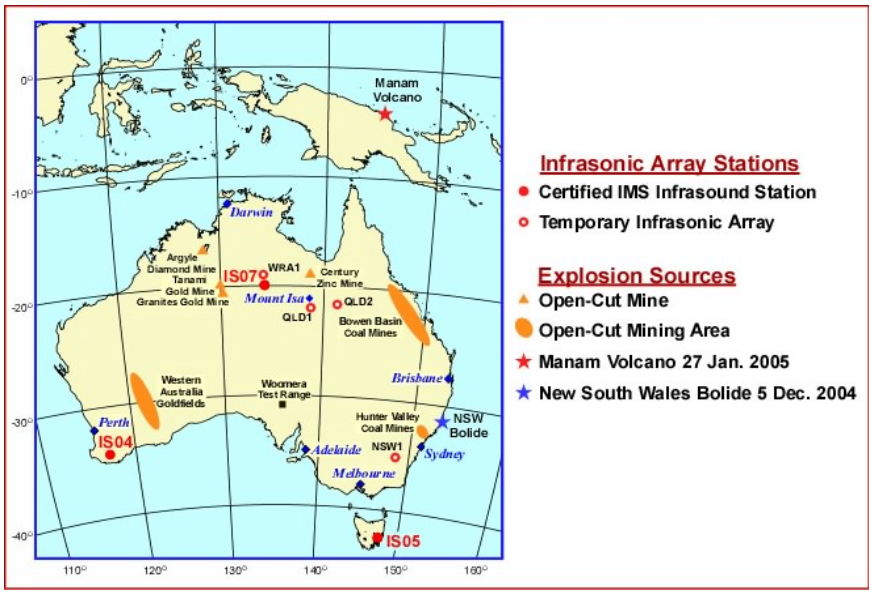


Figure 2. Map of the Australian region showing the locations of certified IMS monitoring stations, the locations of the most significant open-cut mines and open-cut mining regions, the sites of temporary infrasonic arrays, and the locations of the Woomera Test Range, Manam Volcano and the New South Wales bolide.

### 3.1.1. IMS Infrasound Stations in Australia

The three certified IMS stations in Australia, ISO4 Shannon in southwest Australia, IS05 Hobart in Tasmania and IS07 Warramunga in the Northern Territory, are arranged in a roughly equilateral triangle on the Australian continent (see Figure 2). The average separation between these stations is about 2600 km, which is significantly larger than the average station separation distance in the global network (approximately 1970 km). These stations form a local network that effectively monitors the Australian mainland and the area around Australia, including the vast open ocean areas to the west and south of the Australian continent. These stations need to have good monitoring capability for explosions that occur at distance of up to at least 4000 km.

The detection characteristics, array configurations and background noise properties of IS04 Shannon, IS05 Hobart and IS07 Warramunga differ substantially. As can be seen from the array configurations presented in Figure 3, the overall aperture of each of these arrays is approximately the same, but the configurations are completely different. IS07 Warramunga was one of the earliest stations to be established in the IMS infrasound network. In this case, the 8-element array is configured in the form of a "low-frequency" 4-element centered triangle 2-km aperture main array (shown in blue in Figure 3) with a smaller aperture centered triangle "high-frequency" sub-array (shown in red in Figure 3) located in the center of the main array. The array at IS05 near Hobart is configured in the form of a 1.7 km aperture pentagon main array with a small aperture 3-element sub-array located outside the main array. The array configuration at IS04 is again different with a 1.8 km aperture centered triangle main array and a 5-element, roughly pentagon-shaped, small aperture sub-array located on the edge of the main array. The somewhat unusual array configurations at IS04 and IS05 have been installed to accommodate local conditions. The array response for all arrays (see Figure 3) is quite good with fairly reasonable side-lobe suppression. Spatial aliasing will not be a problem except in the case of higher frequency signals with low-signal-to-noise ratios. In this case, the technique developed by Kennett et al. (2003) can be used to minimize spatial aliasing and lower detection thresholds.

Infrasound stations IS04, IS05 and IS07 are located in essentially different environments with substantially different noise characteristics (see Figure 4).

Background noise levels at IS04 are almost always very low. The example of higher noise levels shown in Figure 4 was recorded at IS04 during a storm. In contrast, noise levels at IS05 tend to be fairly high at all of times. The background noise levels at IS07 are generally high during the daytime and usually very low at night. The minimum background noise level at all of these IMS stations at high frequencies is limited by the electronic noise floor of the MB2000 microbarometer sensors that are used at each of these stations. The Chaparral 5.1 infrasonic microbarometer sensor has a much lower electronic noise floor than the MB2000 and measurements made at IS07 show that the minimum noise level at high frequencies is substantially less than the minimum noise level obtained with a MB2000 sensor. An example of the exceptionally low background noise levels at high frequencies recorded at IS07 with a Chaparral 5.1 sensor in zero wind

conditions is shown in Figure 30 in Section 4.3. These observations provide a new low-noise model for the atmosphere at higher infrasonic frequencies.

IS04 is located in the Shannon National Park inside one of the tallest forests in Australia. The tall dense forest at Shannon provides very good shelter from the ambient winds. Microbaroms generated by storms over the Southern Ocean can be detected at all times of day in the data from IS04, including data recorded near noon under conditions of maximum daytime convection.

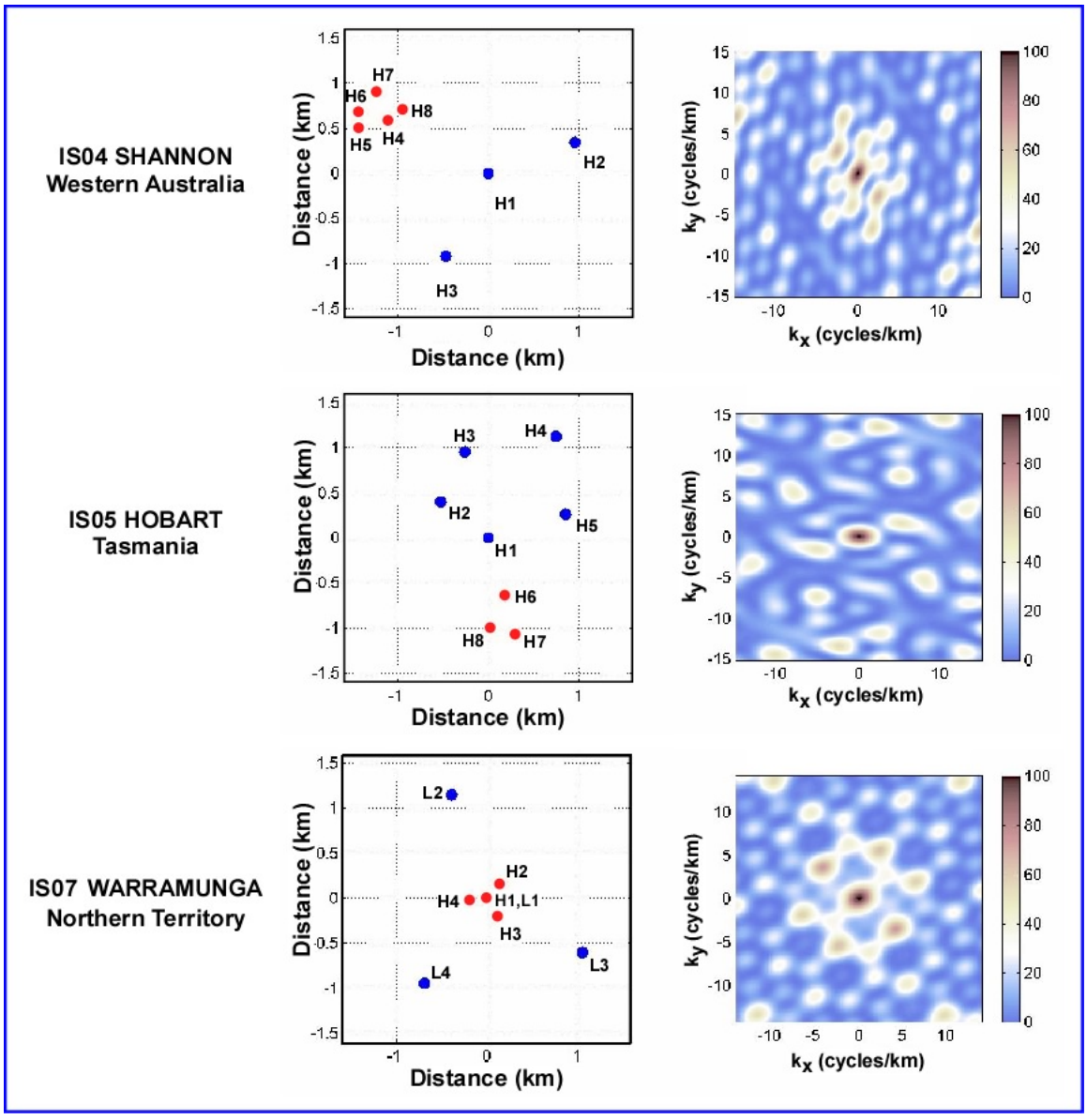


Figure 3. Comparison of array configuration and response at IS04 Shannon, IS05 Hobart and IS07 Warramunga. The elements in the small aperture sub-array in each configuration are shown in red.

It is worth noting that long-period background noise levels at frequencies in the passband from about 0.01 to 0.1 Hz are unusually low at IS04.There are therefore two potentially good monitoring passbands at IS04, one at frequencies of about 0.03 to 0.1 Hz below the microbarom passband and one at frequencies above 0.4 Hz. The monitoring capability at frequencies above 1.5 Hz may be limited on occasion by higher frequency surf-generated noise. Longer period semi-continuous auroral-generated infrasonic signals are also observed at IS04 from time to time. The exceptional low-noise conditions at IS04 suggest that this station will play a valuable role in the monitoring of the open ocean regions in the South Indian and Southern Oceans.

Noise conditions at IS05 in Tasmania are not nearly as good as those found at IS04. This station is located in a fairly open eucalypt forest which provides some shelter from the ambient winds, but noise levels tend to be relatively high at all times of day and to vary significantly from one array element site to the next. The nocturnal inversion at the array site, if any, tends to be weak and intermittent. High frequency noise associated with surf activity along the eastern coast of Tasmania is frequently observed. As with IS04, microbaroms generated by intense storms over the Southern Ocean tend to have high amplitudes, but, in contrast with IS04, microbaroms cannot be detected at all times due to wind-generated background noise.

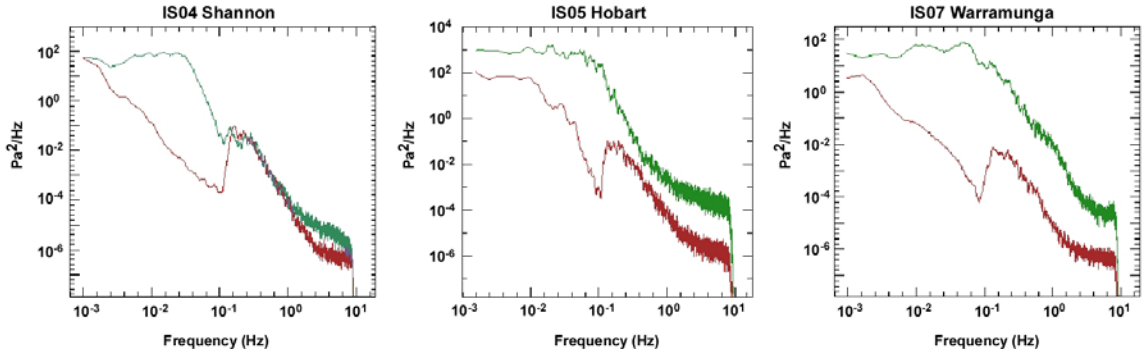


Figure 4. Power spectral density for very low wind noise (dark red) and high wind noise (green) conditions at IS04 Shannon, IS05 Hobart and IS07 Warramunga.

IS07 at Warramunga in the Northern Territory is located in a sparsely vegetated semi-desert environment. Some protection from the ambient winds is provided by long grass, bushes and a few small trees, but wind-noise levels are almost always unacceptably high during the daytime. Winds in the boundary layer are decoupled from the surface shortly after sunset with the rapid development of an intense nocturnal radiation inversion. Noise levels therefore tend to be very low at night except when the radiation inversion is destroyed by thunderstorm activity or by propagating highly nonlinear mesoscale solitary waves and internal bore wave disturbances (Christie, 1989). Highly nonlinear gravity waves of this type are frequently observed at IS07. They also occur on occasion at IS04 Shannon, but only rarely at IS05 Hobart.

The results of the critical examination of the Australian infrasound monitoring stations indicate that IS04 Shannon has very good performance characteristics. This can be attributed to the generally low background noise levels at this station. This survey also

suggests that IS07 at Warramunga is probably, on average, a much better monitoring station than IS05 Hobart. The detection capability for explosion-generated infrasonic waves from distant explosions appears to be significantly greater at IS07 than at IS05. In particular, we note that the vast majority of explosion-generated events detected at IS05 originate on the island of Tasmania. Despite the high frequency of large mining explosions on the Australian mainland, very few of these events have been detected to date at IS05. This is an unexpected result. It may be due to the fact that signals from many sources on the Australian mainland can only propagate to IS05 in a thermospheric waveguide, or it may simply be a manifestation of the background noise conditions at IS05.

### 3.1.2. Field Experiments

A 4-element portable infrasonic array has been assembled, tested and deployed at a number of carefully selected sites on the Australian continent. The portable array infrasonic experiments were designed to:

a) Identify the source of infrasonic signals observed at IMS infrasound stations in the Australian region;
b) Provide data that will help to delineate the various mechanisms that contribute to infrasonic background noise in a wide variety of environments;
c) Test procedures that can be used to minimise the influence of background noise;
d) Provide data that can be used in conjunction with data from existing IMS infrasound stations to delineate the signal coherence properties of explosion-generated infrasound from a wide range of sources at different azimuths and distances under a variety of waveguide conditions.

The sites of the various portable array experiments, along with the locations of the certified Australian IMS stations, are shown in Figure 2. The first portable array experiment (NSW1) was carried out in late February and March 2006 at a site in New South Wales located between the Hunter Valley open-cut coal mining region north of Sydney and infrasound station IS05 Hobart in Tasmania. This experiment was motivated by the observation that very few mining explosions on the Australian mainland are observed at IS05. In contrast, infrasonic waves generated by open-cut mining explosions at mines located at distances of 1000 km or more are observed frequently at IS07. A large number of mining explosions at near and regional distances were recorded during the NSW1 experiment, but none of these events were detected at IS05. The second temporary array (WRA1) was established about 18 km north of IS07 Warramunga in early April 2006. This array was operated for a period of about 6 weeks and with sampling rates of both 20 and 100 Hz. This experiment was designed to identify local infrasound signal and noise sources at IS07. Numerous local sources of small explosions were identified during this experiment, most of which were located around the town of Tennant Creek at a distance of about 40 km from IS07. A short experiment (QLD1) was then conducted near the Mount Isa Mines smelter and the Mica Creek coal-fired power station in western Queensland to see if significant infrasound was being generated by this industrial complex. The results of this experiment indicate that relatively small amplitude

infrasound signals are generated by these installations at frequencies above 2 Hz. It appears that infrasound from these sources will not be detectable at distances beyond 100 km. Finally, a temporary array (QLD2) was established for a six-week period nearly half way between IS07 and the extensive Bowen Basin coal-mining region in eastern Queensland and almost due south of the Century Zinc Mine in far north Queensland. This experiment was designed explicitly to extend the observational database for correlation studies to different distances and different propagation paths.

## 3.2. Portable Infrasonic Array Equipment

A 4-element portable infrasonic array was constructed with a Chaparral Physics Model 5.1 microbarometer located at each array element. In most cases the arrays were deployed in an irregular centered triangle configuration with an aperture of about 300 m. Data was recorded (usually at 20 and 100 Hz) on Refraction Technology 24-bit model 130-01 digital recorders located at each array element. Power is supplied at each array element by a solar power system and time is maintained at each site to within 5 microseconds using independent GPS clocks.

The Chaparral Physics Model 5.1 microbarometer has a particularly low sensitivity to seismic vibrations and the electronic noise floor is several orders of magnitude below that of the MB2000 microbarometer. MB2000 microbarometers are used at all IMS stations in Australia. The microbarometers at each site in the portable array are connected to an efficient wind-noise-reducing system constructed from four 15-m lengths of porous garden hose arranged in a spiral configuration around the microbarometer. Porous hose systems provide effective wind noise reduction and these systems do not usually exhibit unwanted resonances. We have found, however that porous hose wind noise reducing systems do not work if the hose is saturated by rain. The properties of these hoses may also change substantially if they are used in a dusty environment or under conditions where they are immersed in silt-laden groundwater.

## 3.3. Data Processing

All data from infrasound stations IS04 Shannon, IS05 Hobart and IS07 Warramunga and data recorded during the portable array experiments have been processed using a standard automatic signal detection algorithm developed by Dr. David Brown at Geosciences Australia. Signals are identified using pre-set thresholds on both the array-averaged correlation coefficient and the Fisher F-statistic.

The analysis is carried out in 11 overlapping passbands (see Table 1) that span all infrasound frequencies. Passband 4 (0.2 – 0.7 Hz) is used only with array elements in the large aperture sub-array at IMS stations in an attempt to improve detection capability on the high frequency side of the microbarom peak. This procedure can be expected to improve detection for signals from distant explosions since the spatial correlation between array elements in this larger aperture array is reduced for microbarom signals. The longer period passbands centered at frequencies below 0.06 Hz will be of interest from a monitoring perspective only in the case of very large explosions. Infrasonic signals detected in these very long period passbands are of scientific interest, however,

since they include long-period auroral-generated signals, orographically-generated signals and other poorly understood long-period infrasonic signals.

Table 1. Analysis Passbands Used in Routine Data Processing

| | Passband | Comment |
|---|---|---|
| 1. | 1.6 – 7.0 Hz | High-Frequency Passband: Used with high-frequency small aperture sub-array only. |
| 2. | 0.8 – 2.0 Hz | All array elements |
| 3. | 0.4 – 1.2 Hz | Primary monitoring passband. All array elements. |
| 4. | 0.2 – 0.7 Hz | Used with large-aperture 4-element sub-array only |
| 5. | 0.1 – 0.5 | Microbarom passband. All array elements |
| 6. | 0.06 – 0.1 Hz | Long-period monitoring passband. All array elements. |
| 7. | 0.03 – 0.07 Hz | All array elements |
| 8. | 0.016 – 0.033 Hz | All array elements |
| 9. | 0.007 – 0.02 Hz | All array elements |
| 10. | 0.002 – 0.007 Hz | All array elements |
| 11. | 0.0017 – 0.004 Hz | All array elements |

All data recorded to date at IMS infrasound stations IS04, IS05 and IS07, including the very large archived data set from IS07 has been processed. The starting date for each IMS station data set is given in Table 2. This analysis has resulted in the detection of a very large number of infrasonic signals, including signals from local, regional and distant mining explosions, earthquake-generated infrasonic signals, aircraft-generated signals, signals from volcanic explosions, bolide-generated signals, continuous monochromatic signals of unknown origin, signals from industrial activity, microbaroms generated by intense storms over the Southern Ocean, tropical cyclones off the east and west coasts of Australia and typhoons north of Papua-New Guinea, orographically-generated infrasound and auroral-generated infrasound.

Table 2. Operational Starting Date for IMS Infrasound Stations in Australia

| Station | Operational Starting Date |
|---|---|
| IS04 Shannon | 01 April 2006 |
| IS05 Hobart | 01 July 2004 |
| IS07 Warramunga | 21 March 2001 |

## 4. RESULTS AND DISCUSSION

As noted in the Introduction, the work carried out during this project has identified three potentially serious problems that may limit detection capability at IMS infrasound stations:

a) Problems associated with the loss of higher frequency signal components in the primary monitoring passband,

b) Detection problems associated with a low degree of signal coherence between array elements and

c) Problems with high levels of wind-generated background noise.

These problems and proposed solutions to these problems are discussed in the following sections.

## 4.1. Decay of Higher Frequency Infrasonic Signal Components

The establishment of the International Monitoring System (IMS) for verification of the Comprehensive Nuclear-Test-Ban Treaty has led to an emphasis on the detection of small nuclear explosions with yields of less than a few kilotons. Since the dominant frequency of infrasonic waves observed from smaller nuclear explosions at distances comparable to the average separation of stations in the IMS network is relatively high, there has been a tendency in recent years to focus only on the detection of explosion-generated infrasonic waves at high frequencies (> 0.5 Hz) only. The initial work in this project showed that the detection of longer-period thermospheric infrasound components from regional and distant explosions should not be ignored. Indeed, good detection capability at frequencies both above and below the microbarom passband is essential to ensure that atmospheric nuclear explosions at any place on the globe can be reliably detected and located by the 60-station IMS infrasound monitoring network. In some circumstances, longer period thermospheric components may be the only detectable waves observed at an infrasound monitoring station. Even if the higher frequency stratospheric components are detected, the detection of a thermospheric phase provides additional information that can be used to reduce source location error estimates. Good detection capability for longer period thermospheric infrasound is essential for the reliable monitoring of the vast open ocean regions in the Southern Hemisphere.

A good example of the need for good detection capability at long periods is provided by observations of signals at IS05 Hobart from the explosive eruption of Manam volcano located near the northern coast of Papua New Guinea (see Figure 2) on January 27, 2005. In the case of the Manam volcano eruption, the only signals observed at IS05 at a distance of 4261 km were long-period (0.01 to 0.1 Hz) thermospheric infrasonic waves. All high frequency signals were eroded away completely along the essentially meridional propagation path between Manam Volcano and the IS05 array. In contrast, both high frequency stratospheric signals and low frequency thermospheric signals were detected at IS07 Warramunga at a distance of 2103 km. Record sections showing the low-frequency infrasonic signals observed at IS05 and the high-frequency and low-frequency observations at IS07 are shown in Figures 5 and 6 respectively. A series of bandpass filtered signals spanning the frequency range from 0.03 Hz to 9.0 Hz is shown in Figures 7 and 8 for data recorded at IS05 and IS07. As can be seen from these examples, signals with large signal-to-noise ratios were observed at both IS05 and IS07 at low frequencies. However, stratospheric signals with frequencies above 0.1 Hz were not detected at IS05. It is interesting to note that signals from Manam volcano were detected in routine automatic processing of data from IS07 at frequencies of up to at least 2.0 Hz. Signals at IS07 were also detected at frequencies in the microbarom passband between 0.06 and 0.1

Hz. A careful examination of the Manam volcano data recorded at IS07 shows that very high frequency signals with significant energy content were recorded at frequencies of up to at least 5 Hz. However, the degree of signal correlation between the array elements at IS07 for signals with frequencies above 2.0 Hz is very small. This potentially serious problem is discussed in detail in Section 4.2. Signals from the Manam eruption were also recorded at several other distant IMS arrays (Campus et al., 2005) and in almost all cases, these distant observations were also restricted to long-period thermospheric waves.

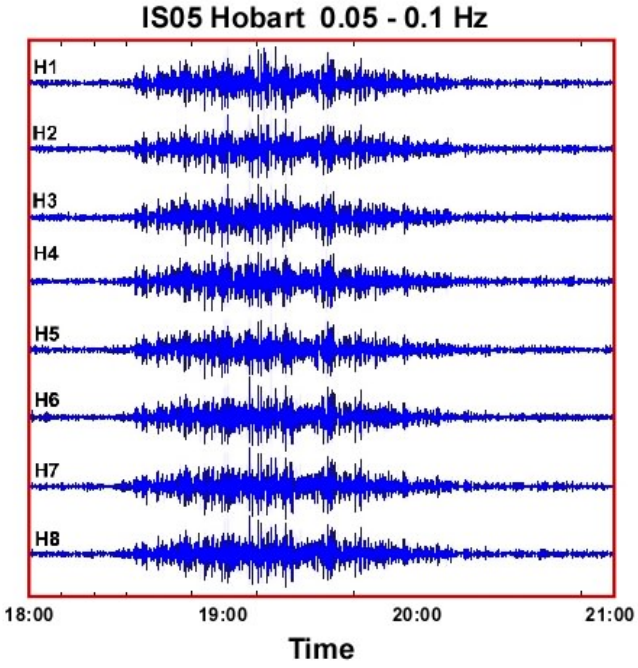


Figure 5. Low-frequency (0.05 to 0.1 Hz) thermospheric infrasonic signals observed at IS05 Hobart from the explosive eruption of Manam Volcano on 27 January 2005.

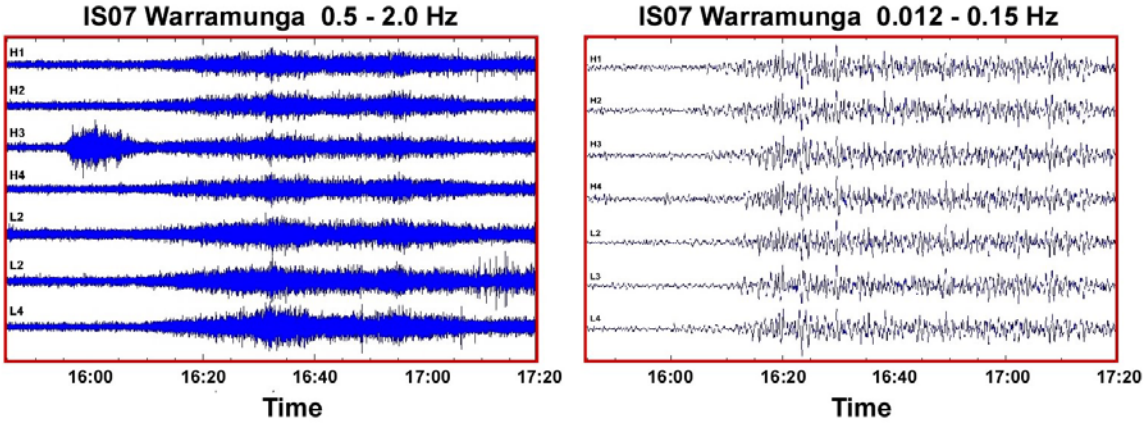


Figure 6. High frequency and low-frequency infrasonic signals observed at IS07 Warramunga from the explosive eruption of Manam Volcano on 27 January 2005.

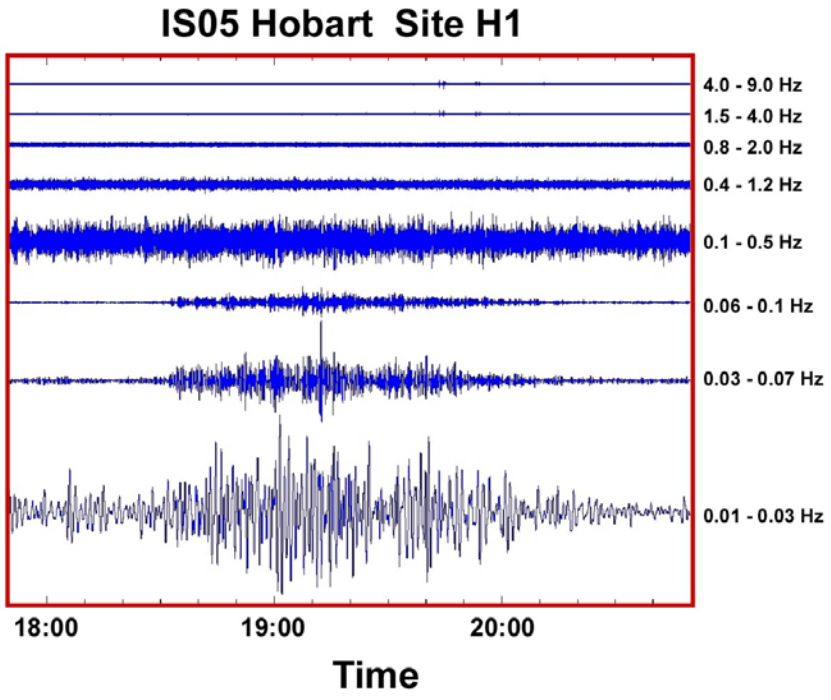


Figure 7. Bandpass filtered signals observed at IS05 Hobart from the explosive eruption of Manam Volcano on 27 January 2005.

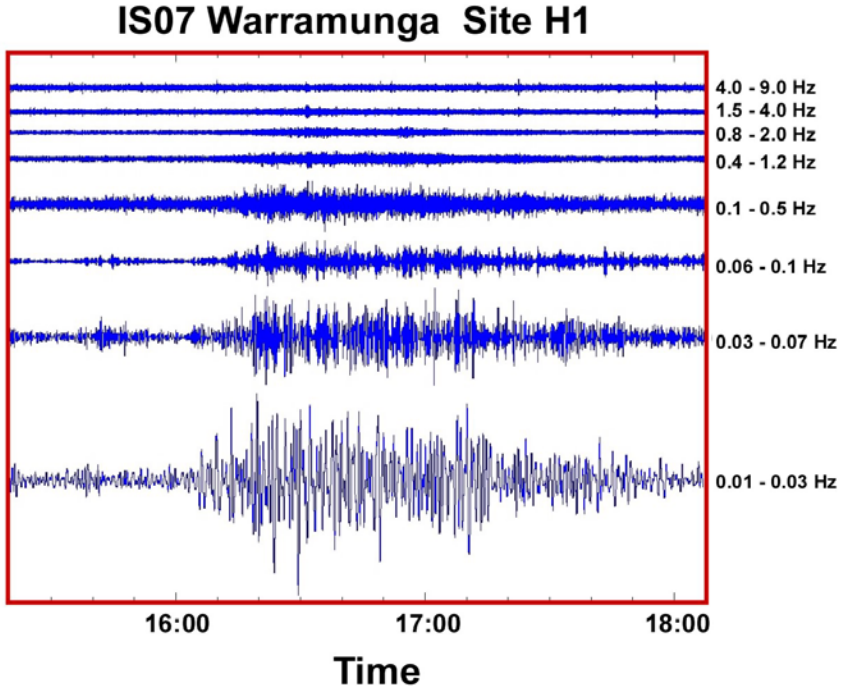


Figure 8. Bandpass filtered signals observed at IS07 Warramunga from the explosive eruption of Manam Volcano on 27 January 2005.

A second example of the detection of longer period signals from an atmospheric explosion is provided by observations at IS05 and IS07 of infrasonic waves generated by a spectacular bolide that was visually observed along the southeast margin of Australia at about 04:15 AM local time (18:15 UT) on Dec. 5, 2004. The event was located over the New South Wales coast at about 31.7 °S, 152.6 °E, roughly halfway between Port Macquarie and Taree (see Figure 2). Higher frequency stratospheric signals generated by this bolide explosion were observed at both IS05 and IS04. In contrast with the observations at IS07, delayed long period thermospheric signals were also observed at IS05 at frequencies below 0.1 Hz. No signals were detected in the microbarom passband (0.1 to 0.5 Hz) at IS05.

The high-frequency stratospheric waves and delayed low frequency thermospheric waves observed at IS05 Hobart are illustrated in Figure 9. The high- and low-frequency observations of the New South Wales Bolide at IS07 Warramunga are shown in Figure 10. Long-period waves with frequencies below 0.1 Hz cannot be seen in the long-period record section and this is verified by the complete lack of detections at frequencies below 0.1 Hz in the routine processing of data from IS07. Reports in the media indicate that the New South Wales bolide was accompanied by a number of separate audible explosions. This may account for the observed morphology of the signals shown in Figures 9 and 10.

The frequency content of the observed bolide signals at IS05 and IS07 is shown in greater detail in Figures 11 and 12. As in the case of infrasound detections of the Manam explosion at IS05, the high level of background noise due to coherent microbaroms precluded any detection of signals in the passband from 0.1 to 0.5 Hz. The presence of signals can be seen in the 0.1 to 0.5 Hz filtered data shown in Figure 12 for IS07 and these signals were easily detected during the automatic processing of data from this station.

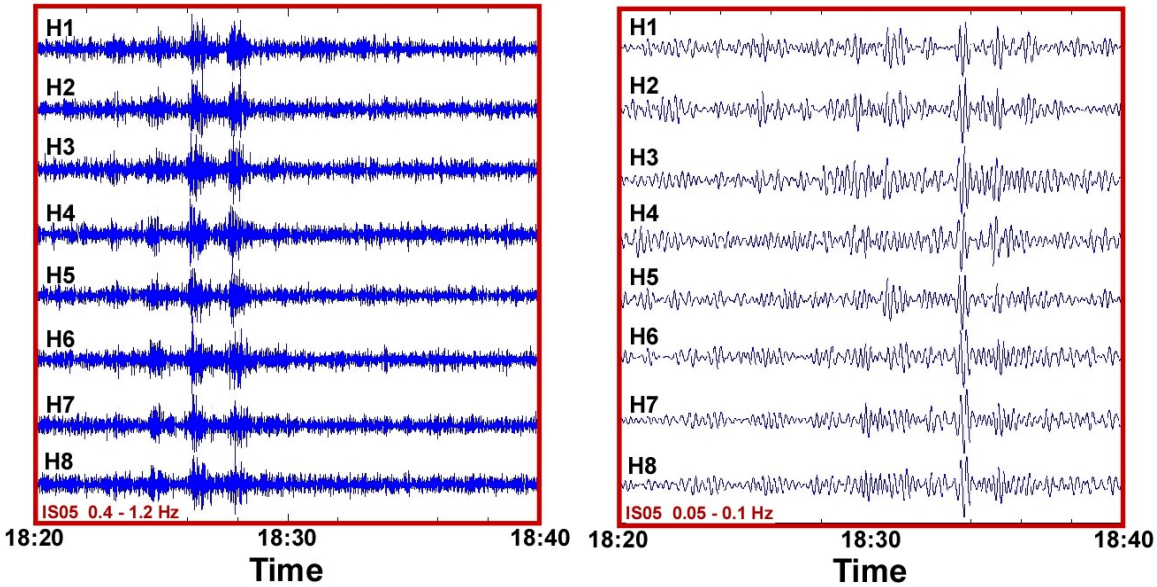


Figure 9. High-frequency and low-frequency observations at IS05 Hobart of the New South Wales bolide on Dec. 5, 2004. The distance to the station is 1270 km. All long-period signals recorded after 18:32 are thermospheric signals.

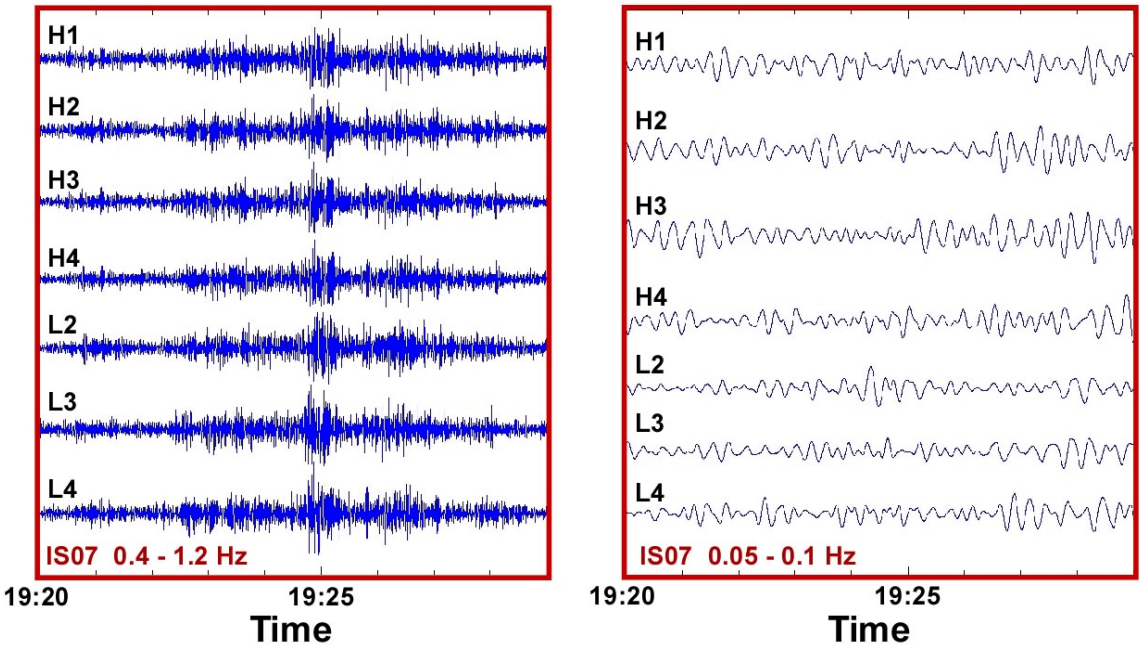


Figure 10. High- and low-frequency observations of the New South Wales bolide on Dec. 5, 2004 at IS07 Warramunga. The distance to the station is 2260 km. Long-period waves with frequencies of less than 0.1 Hz were not detected at IS07.

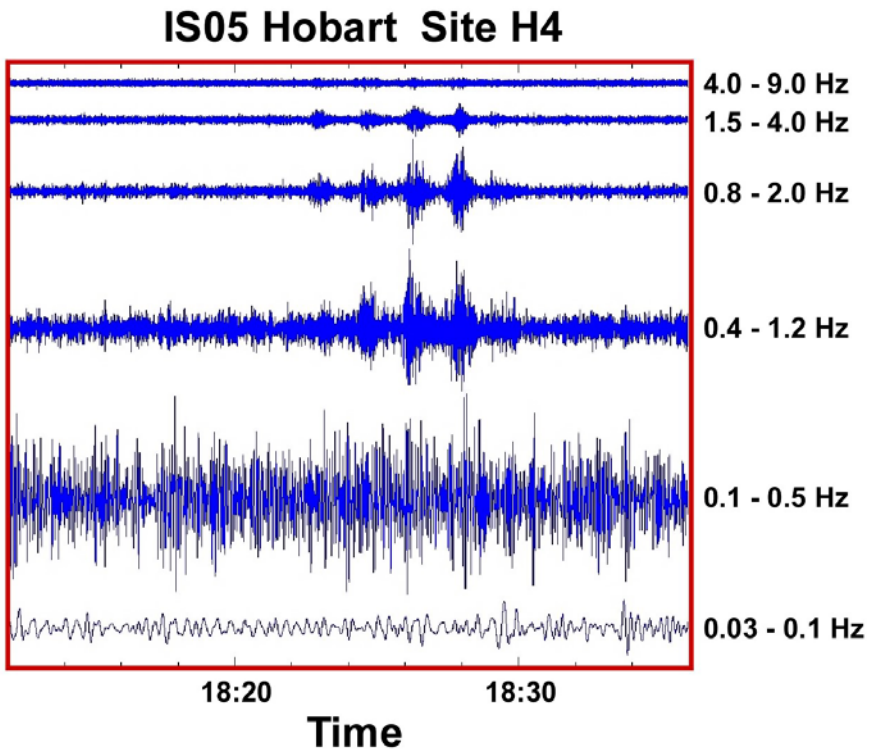


Figure 11. Bandpass filtered signals recorded at IS05 Hobart from the New South Wales bolide on Dec. 5, 2004. The weak thermospheric signals recorded in the 0.03 to 0.1 Hz passband are highly coherent over the array.

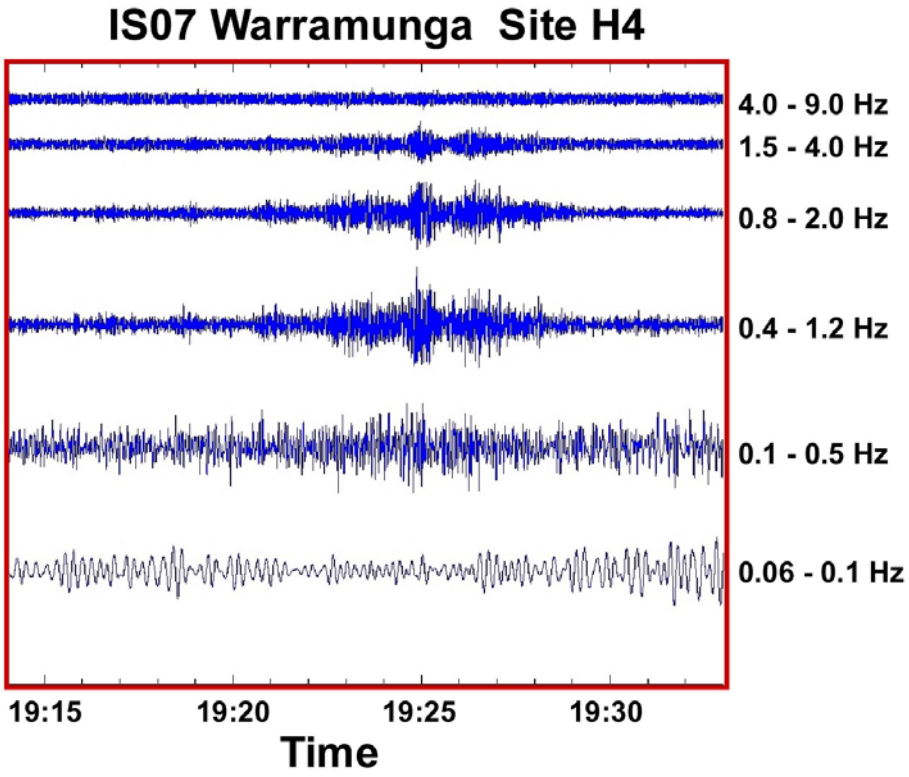


Figure 12. Bandpass filtered signals from the New South Wales bolide on Dec. 5, 2004 recorded at IS07 Warramunga.

The higher frequency signals observed at IS05 at a distance of 1270 km from the New South Wales bolide are predominately stratospheric with a trace velocity of about 348 m/s. These signals are incoherent between array elements in the large aperture pentagon sub-array at IS05 at all frequencies above 0.5 Hz. The low frequency ($f < 0.1$ Hz) signals detected at IS05 are dominated by delayed coherent thermospheric signals with a trace velocity of about 380 m/s. The higher frequency stratospheric signals observed at IS07 at a distance of 2260 km are also incoherent between elements in the large-aperture centered-triangle L array at IS07.

The observations presented above show that the higher frequency components in explosion-generated infrasonic signals decay fairly rapidly with distance from the source and may not be detectable at frequencies above 0.1 Hz at distances that are comparable with distances between stations in the global IMS infrasound monitoring network. The spectral content of signals in this distance range will depend strongly on prevailing atmospheric waveguide conditions and on the distance from the source. It is clearly essential to ensure that routine data analysis procedures include a search for longer period signal components at frequencies below the microbarom passband. These initial observations also emphasize the need for a good understanding of the spatial correlation properties of infrasonic waves generated by regional and distant explosions.

The essential conclusions that can be drawn from this initial investigation are:

a) Higher frequency infrasonic signal components from atmospheric explosions decay fairly rapidly with distance. Observations of distant explosions may be limited to longer period components when propagation is restricted to a thermospheric waveguide;
b) The optimal detection passband will depend on the distance to the source;
c) Detection capability for higher frequency signal components from distant explosions may be significantly reduced by the loss in signal coherence between array elements;
d) Automatic routine signal processing for the monitoring of explosions should be carried out in passbands that span the complete frequency range from 0.01 Hz and 2.0 Hz;
e) All infrasonic phases, including longer period thermospheric phases should be detected and used in location and discrimination algorithms.

## 4.2. Signal Correlation and Optimal Infrasonic Array Design

The results described in Section 4.1 for observations of infrasound from the Manam explosive eruption on 27 January, 2005 and the New South Wales bolide on Dec. 5, 2004 indicate that the small degree of signal correlation between array elements at frequencies above 0.5 Hz may limit the detection of small nuclear explosions when automatic processing of infrasonic array data is based on correlation algorithms. This problem is illustrated in Figure 13 for infrasonic signals recorded at IS07 from the Manam Volcano explosion with frequencies in the passband from 0.8 to 2.0 Hz.

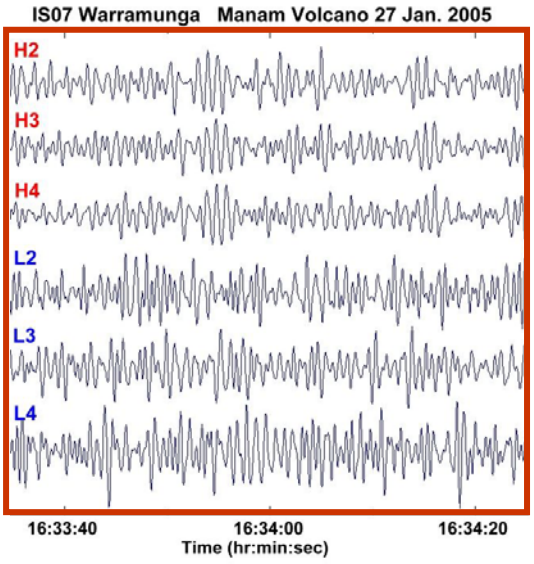


Figure 13. Comparison of highly correlated signals from the Manam Volcano explosion on 27 January 2005 recorded at sites in the small aperture H-array at IS07 with uncorrelated signals recorded at sites in the large aperture L array. Data has been bandpass filtered between 0.8 and 2.0 Hz.

As can be seen from Figure 13, the high-frequency signals recorded at a distance of 2103 km from the Manam Volcano explosion have a fairly high degree of correlation between elements in the small aperture H-array and a much smaller degree of correlation between elements in the large aperture L-array. Array sites H2, H3 and H4 in the small aperture sub-array are separated by about 380 m. Sites L2, L3 and L4 in the large aperture array are separated by about 2 km. In this case, automatic signal detection using correlation techniques is essentially limited to data recorded on the small aperture sub-array. The addition of the central element H1 significantly improves the detection capability of the small aperture sub-array in the 0.8 to 2.0 Hz passband.

It might be expected that the degree of signal correlation between array elements from explosion sources that lie at near regional distances from the monitoring array would be much larger than the degree of correlation observed for sources that lie at distances of more than 2000 km. We have found, however, that the degree of signal correlation between array elements may also be significantly attenuated even when the source lies at distances of less than 500 km. This is illustrated in the high-frequency bandpass filtered data shown in Figure 14 for infrasonic waves generated by a mining explosion located at a distance of 482 km from IS07. The degree of signal correlation is fairly high (> 0.8) between elements in the small aperture (380 m) sub-array (H1, H2, H3 and H4) and fairly low (< 0.5) between all elements in the large aperture (2.0 km) sub-array (L2, L3, L4).

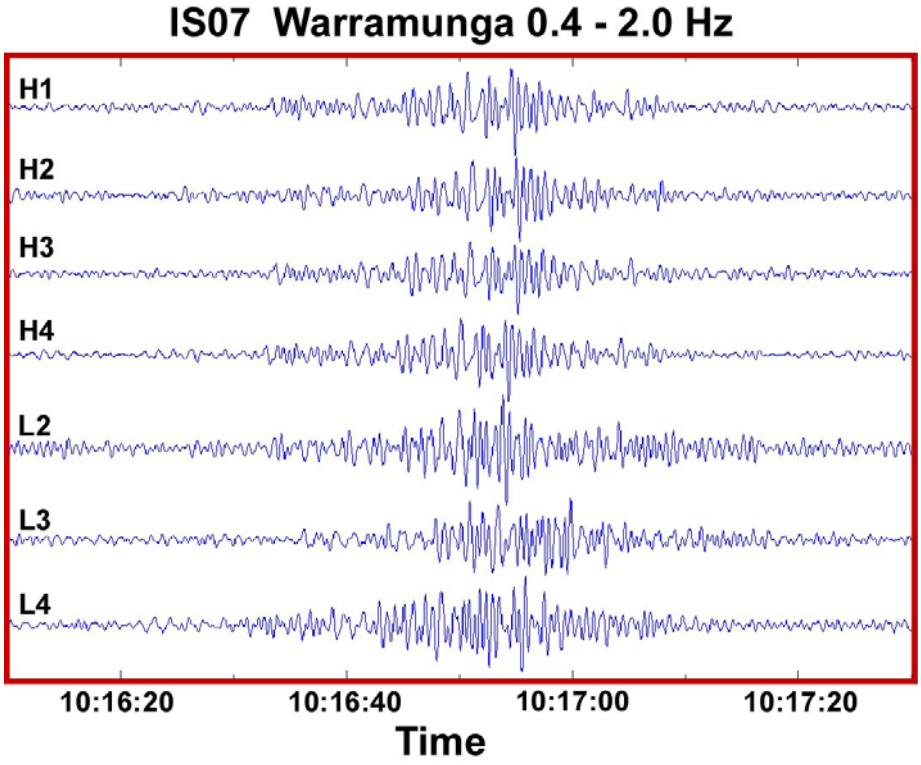


Figure 14. Coherent (H-array) and incoherent (L-array) infrasonic signals observed on 20 September 2002 at IS07 from an open-cut explosion at the Granites Gold Mine. Data has been bandpass filtered between 0.4 and 2.0 Hz. The distance to the source is 482 km.

It seems clear that the optimal design of an infrasonic monitoring array will depend critically on a good understanding of the properties of infrasonic signal correlation as a function of frequency and distance between the array elements. The spatial coherence of infrasonic signals has been studied extensively since the pioneering work of Gossard (1969), Gossard and Sailors (1970) (see also Gossard and Hooke, 1975) and Mack and Flinn (1971). Mack and Flinn (1971) have provided convincing evidence to show that the observed loss of signal coherence along the direction of wave propagation is due to a small variation, $\pm\Delta c$, in the velocity of the waves while the observed loss of coherence along the wavefront is due to a small variation, $\pm\Delta\theta$, in the azimuth of the waves. The coherence parameters $\Delta c$ and $\Delta\theta$ may be frequency and range dependent and the loss in coherence parallel to the wavefront is significantly greater than the loss in coherence normal to the wavefront. This relatively simple model captures the essential physics of the subject and will be adopted here. The physical processes that give rise to spatial decorrelation of infrasonic signals remain poorly understood. It seems reasonable to assume that decorrelation is mainly due to propagation effects associated with wave propagation through an inhomogeneous medium with turbulence and/or small-scale variations in wind speed.

Mack and Flinn (1971) compared model predictions with observations of relatively long-period infrasound generated by large distant nuclear explosions. Blandford (1997, 2000, 2004) extended the work of Mack and Flinn to higher frequency infrasound and further studies have been reported by Armstrong (1998), McCormack (2002), and Christie et al. (2005a, 2006, 2007). Observations of signal correlation between sensors aligned roughly parallel and perpendicular to the wavefront were used by Mack and Flinn to determine the model parameters Δc and Δθ. Blandford's parameters for higher frequency infrasound differ slightly from those found by Mack and Flinn. Typically, for large distances, Δc = 15 m/s and Δθ = 5º (Blandford, 1997). However, there is some uncertainty in the choice of Δc and Δθ since the observations exhibit considerable scatter.

The model of Mack and Flinn (1971) is based on the assumption that the signal is described for a given frequency, f, by a normalized uniform distribution, $F(\mathbf{k},f)$, defined by the window $\pm\Delta c$ and $\pm\Delta\theta$ in frequency-wavenumber space. Integrating the spatial Fourier transform of the wavenumber spectrum $F(\mathbf{k},f)$ over the area where $F(\mathbf{k},f) \neq 0$, and normalizing the result to unity when $|\mathbf{r}| = 0$, gives an expression at frequency, f, for the coherency, γ, and correlation, C, between two sensors separated by vector $\mathbf{r}$, which can be written in the form:

$$C(\mathbf{r},T) = \sqrt{\gamma^2(\mathbf{r},T)} = \sqrt{\left|\frac{\sin\left(2\pi x \sin(\Delta\theta)/cT\right)}{2\pi x \sin(\Delta\theta)/cT}\right|^2 \cdot \left|\frac{\sin\left(2\pi y \Delta c/(cT(c+\Delta c)\right)}{2\pi y \Delta c/(cT(c+\Delta c)}\right|^2} \qquad (1)$$

Here, $T$ is period, $c$ is the mean phase velocity, $\gamma^2$ is squared coherence, Δc and Δθ are model parameters for the deviations in velocity and azimuth, and $x$ and $y$ are the components of the vector separation, $\mathbf{r}$, of the infrasound sensors. Mack and Flinn note that more realistic $F(\mathbf{k},f)$ distributions can be used to define wave amplitudes that gradually reduce to zero from a central maximum, but the results obtained using these

distributions are essentially the same as those described by expression (1). The Mack and Flinn model predicts that signal correlation will depend only on Δc when sensors are aligned normal to the wavefront and only on Δθ when sensors are aligned parallel to the wavefront when Δc and Δθ are small.

Expression (1) can be plotted for y = 0 and constant T to give the Mack and Flinn limiting curve for the variation of correlation between two sensors as a function of sensor separation for sensors aligned parallel to the wavefront. Similarly, a plot of expression (1) with x = 0 and constant T gives the Mack and Flinn limiting curve for the variation of correlation as a function of sensor separation for sensors aligned normal to the wavefront. Examples that illustrate these two limiting curves are shown in Figure 15 for 0.5, 1 and 2 Hz infrasonic waves. This figure is adapted, in part, from Blandford (2000) and includes data from two different shuttle launches recorded at DLIAR (2500 km) and IS10 Lac du Bonnet (2800 km). The Mack and Flinn limiting curves shown here are calculated for $\Delta c$ = 12, 15 and 18 m/s and $\Delta\theta$ = 5º, 6º and 7º. As can be seen from this Figure, signal correlation between two array elements is strongly dependent on the separation between the elements and on the frequency of the wave. The data illustrated in Figure 15 for periods of 0.5 and 1.0 seconds exhibit considerable scatter, but the overall trends are clear. The degree of signal correlation between sensors decreases rapidly as sensor separation increases and as frequency increases. In addition, the degree of signal correlation depends strongly on the alignment of the sensors with respect to the wavefront at large sensor spacing or at high frequencies. The parameters adopted by Blandford (2000), $\Delta c$ = 15 m/s and $\Delta\theta$ = 5º, provide a reasonably good fit to the data, but they may be slightly too restrictive. We shall however continue to use Blandford's parameters in the correlation calculations presented below.

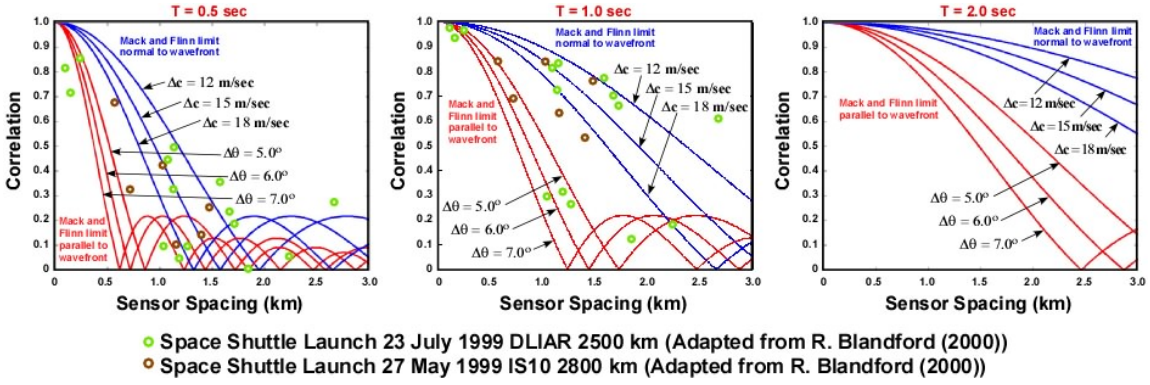


Figure 15. Correlation of 0.5, 1.0 and 2.0 Hz infrasonic signals parallel and perpendicular to the wavefront as a function of sensor spacing (adapted in part from Blandford (2000)).

The Mack and Flinn model provides a good description of the observed decrease in signal correlation between two infrasonic sensors as the distance between the sensors is increased, the dependence of correlation on sensor pair orientation with respect to the wavefront, and the rapid decrease in correlation with increasing frequency. In view of the simplified representation, $F(\mathbf{k},f)$, used in the derivation of the Mack and Flinn model to model the distribution of waves in the wavenumber domain, it must be expected that the model will only provide an approximate fit to signal correlation observations. However,

the functional form of expression (1) does provide a reasonable description of all observed signal correlation properties.

The comparison of data illustrated in Figure 15 is an example of the traditional method that has been used in the past to compare infrasonic wave coherence observations with theory. This method works well when it is possible to find pairs of array elements separated by a range of distances and aligned both along and perpendicular to the wavefront. The method is less useful when the array contains a small number of array elements where few, if any, array element pairs are aligned normal and perpendicular to the wave propagation direction. We have therefore decided to use a different comparison method that can be applied directly to any array configuration and which includes implicitly a contribution from all array element pairs. The method, which is based on the use of the predicted azimuthal variation of the array-averaged correlation coefficient, also allows the model predictions at a specified frequency to be compared directly on the same plot with observed infrasonic wave correlation data corresponding to sources located at any azimuth.

An important feature of the predicted array-averaged correlation coefficient distribution is that this polar distribution provides a unique array characteristic, which can be used to measure array performance. This then provides a basis for the design of an optimal infrasonic array.

Consider first the azimuthal variation of the signal correlation between two sensors as predicted by the Mack and Flinn model. The predicted azimuthal variation as defined by expression (1) is plotted in Figures 16 in polar coordinates as a function of both sensor separation distance and wave period. These curves have been calculated with the same parameters as those used by Blandford (2000) and the results at the extremes can be compared with the limiting Mack and Flinn curves shown in Figure 15.

The curves shown in Figure 15a correspond to a sensor separation of 1.0 km. In this case, the azimuthal variation of the predicted correlations is almost isotropic when the period exceeds 2.0 seconds, although the maximum reduction in correlation along the wavefront direction is still significant for T = 2.0 seconds. The degree of anisotropy in the azimuthal distribution increases rapidly as period decreases below 2.0 seconds. This indicates that the dominant contribution to the overall array-averaged correlation coefficient at higher frequencies will come from array element pairs that are aligned more or less in the wave propagation direction and suggests that some array configurations may exhibit azimuthally-dependent detection characteristics. This will be illustrated further in the results presented below.

The results illustrated in Figure 16b for the azimuthal variation of the correlation between two sensors as a function of sensor spacing are similar in form to those shown in Figure 16a. The azimuthal distribution is essentially isotropic at a frequency of 1 Hz when the sensor separation distance is less than about 0.3 km and highly anisotropic when the separation is more than about 1.0 km. Again these results suggest that certain array configurations may exhibit detection characteristics that are azimuthally biased at higher frequencies.

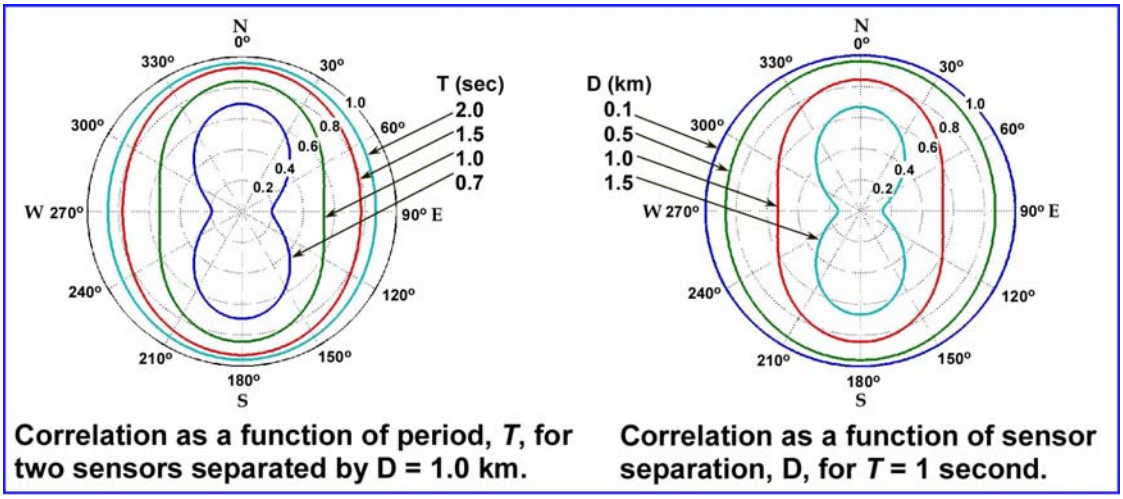


Figure 16. Predicted azimuthal variation of signal correlation between two sensors as a function of a) wave period, T, and b) station separation, D. $\Delta c$ = 15 m/s and $\Delta\theta$ = 5º.

The predicted degree of correlation between any pair of sensors in an array with a separation vector **r** for infrasonic waves from all azimuths is specified, at a given frequency, by expression (1). Thus, the predicted correlations for all wave back-azimuths can be calculated for each individual sensor pair in the array in a common geographic coordinate system where the wave back-azimuth is measured from north. The results for each sensor pair can be then be averaged over the array to give a predicted normalized array-averaged correlation coefficient for all wave back-azimuths. The resulting polar distribution of the array-averaged correlation coefficient is thus a unique characteristic of the array configuration, the parameterization of Mack and Flinn theory, and the specified frequency. As noted above, each sensor pair in the array contributes to the predicted array-averaged correlation coefficient for any wave back-azimuth direction and thus the observed normalized array averaged correlation coefficients from all sources can be plotted on the same diagram and compared directly with the theoretical predictions.

In order to illustrate this procedure, we focus initially on the predicted results for arrays with a small number of array elements in order to emphasize potential problems with the reliable detection of infrasonic signals from regional and distant explosions. More specifically, we choose for illustration the following tripartite sub-arrays from IMS infrasound station IS07 Warramunga (see Figure 3):

a) A large aperture (about 2.0-km) array defined by array elements L2, L3 and L4,
b) A medium aperture (about 1.5 km) array defined by array elements H2, L3 and L4 and
c) A small aperture (about 0.3 km) array defined by array elements H2, H3 and H4.

This procedure allows us to compare directly the theoretical predictions of the array-averaged correlation coefficient for sparse arrays with array averaged signal correlations of infrasonic signals observed at IS07. The predicted azimuthal distributions of the array-averaged correlation coefficients for this set of sub-arrays at IS07 at three different frequencies along with the specific sub-array configurations are shown in Figure 17.

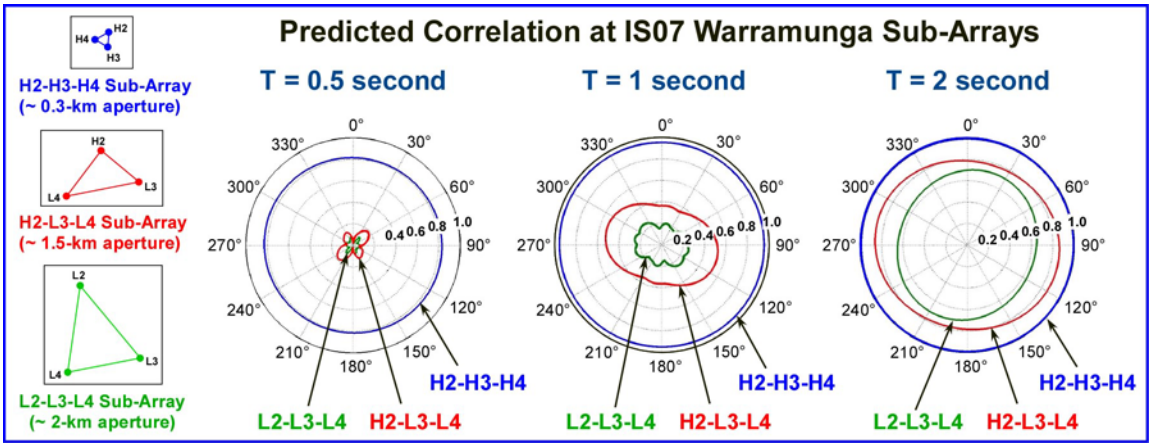


Figure 17. Predicted azimuthal variation of the array-averaged correlation coefficient for a large-aperture (~2 km) sub-array (in green), a medium aperture (~1.5 km) sub-array (in red) and a small aperture (~0.3 km) sub-array (in blue) at IS07 Warramunga, Australia. Azimuth is measured from north. The calculations are based on $\Delta c = 15$ m/s and $\Delta\theta = 5°$ as found by Blandford (1997).

As noted above, the azimuthal distribution of the array-averaged correlation coefficient provides a unique characteristic of the array configuration, which can be used to assess array detection capability. The results presented in Figure 17 show that the array-averaged correlation coefficient for sparse arrays may be strongly anisotropic at higher frequencies when the array aperture is large. The results also indicate that regional and distant explosions may not be detected reliably on larger aperture triangular arrays at frequencies above 1 Hz.

Examples of the comparison between signal correlation observations and model predictions for the large-, medium- and small-aperture sub-arrays at IS07 are shown in Figures 18a, 18b, 19a, and 19b for both naturally-occurring distant explosions and regional and distant mining and other chemical explosions.

The observations shown in Figures 18 and 19 are in fairly good agreement with model predictions. Observed signal correlation decreases rapidly with increasing frequency and with increasing array aperture in agreement with theory. The observations confirm that the degree of signal correlation of infrasound from regional and distant explosions is very low on sparse arrays with apertures of about 1 km or more at frequencies above 1 Hz. The degree of signal correlation will also be unacceptably small at all frequencies in the primary monitoring passband (0.4 to 1.2 Hz) if the array aperture exceeds 2 km.

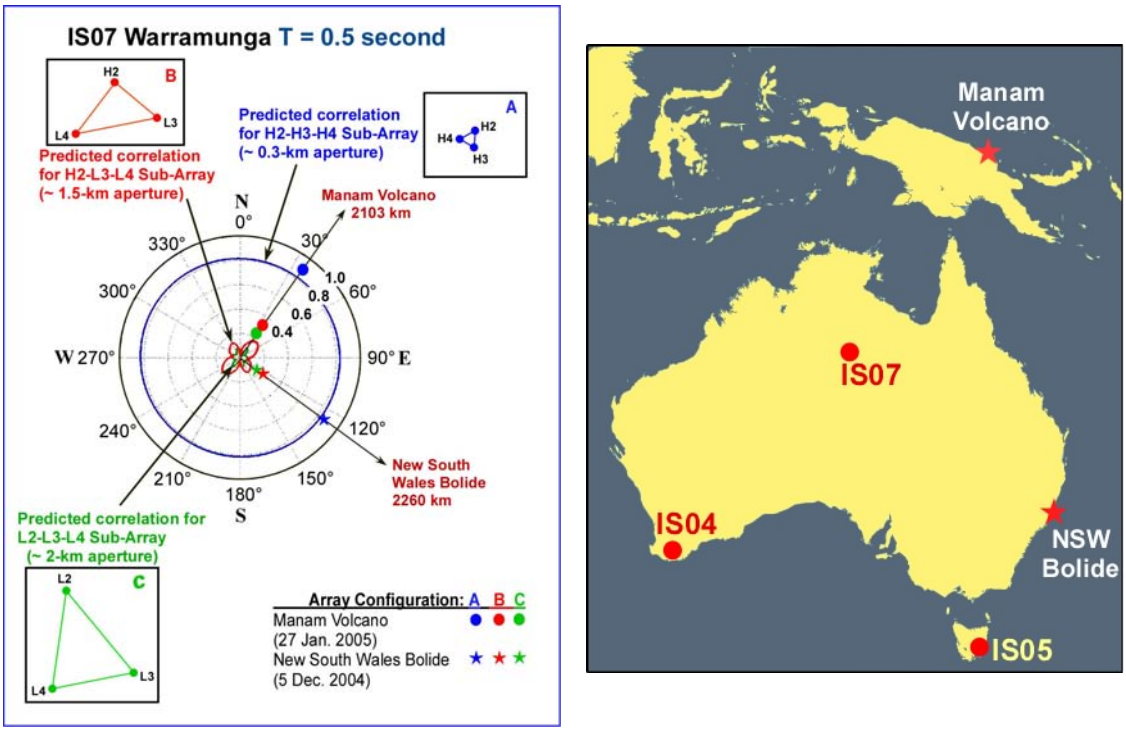


Figure 18a. Comparison of predicted and observed array-averaged correlation coefficients for 2.0 Hz infrasonic signals from distant volcanic and bolide explosions recorded on small, medium and large aperture sub-arrays at IS07 Warramunga.

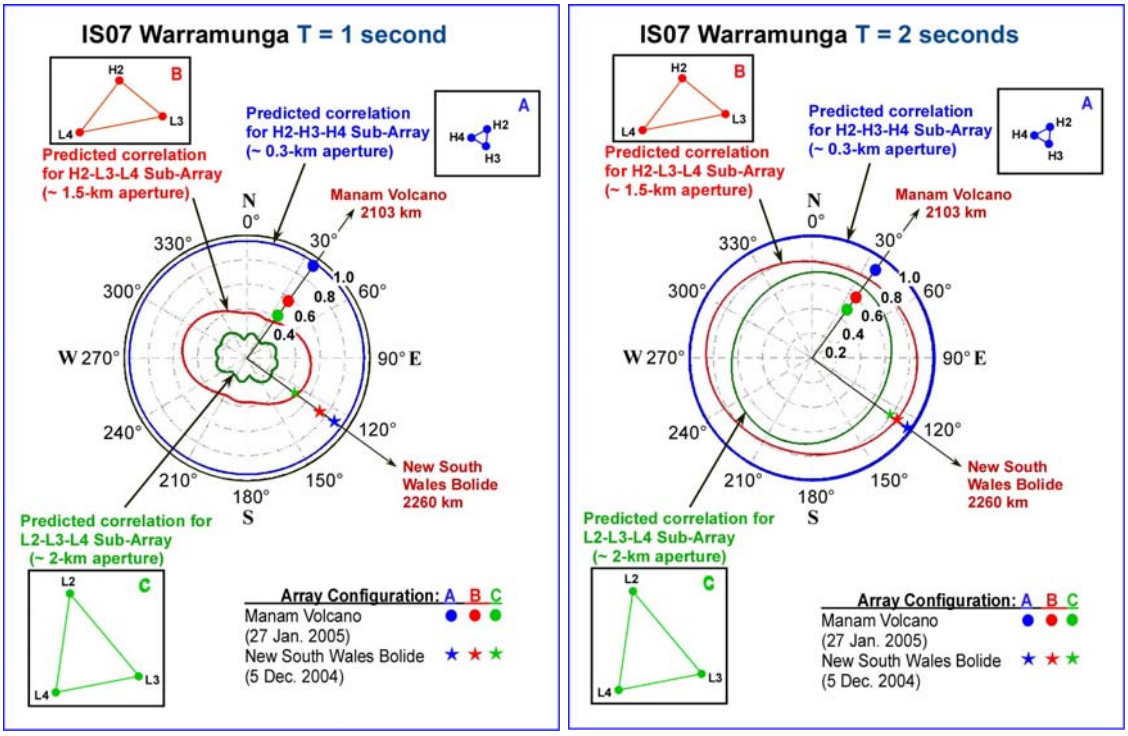


Figure 18b. Comparison of predicted and observed array-averaged correlation coefficients for 0.5 and 1.0 Hz infrasonic signals from distant volcanic and bolide explosions recorded on small, medium and large aperture sub-arrays at IS07.

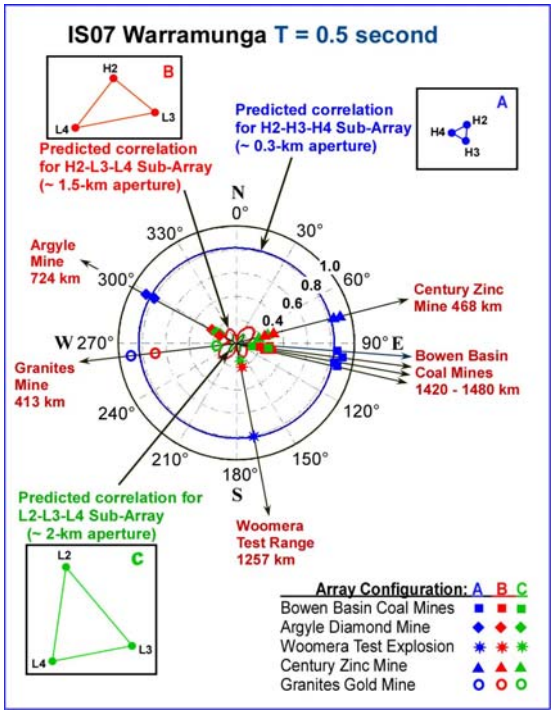


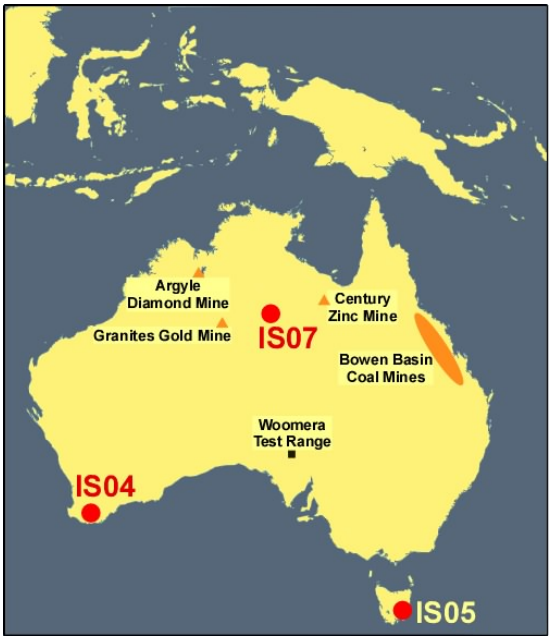


Figure 19a. Comparison of predicted and observed array-averaged correlation coefficients for 2.0 Hz infrasonic signals from regional mining and other chemical explosions recorded on small, medium and large aperture sub-arrays at IS07.

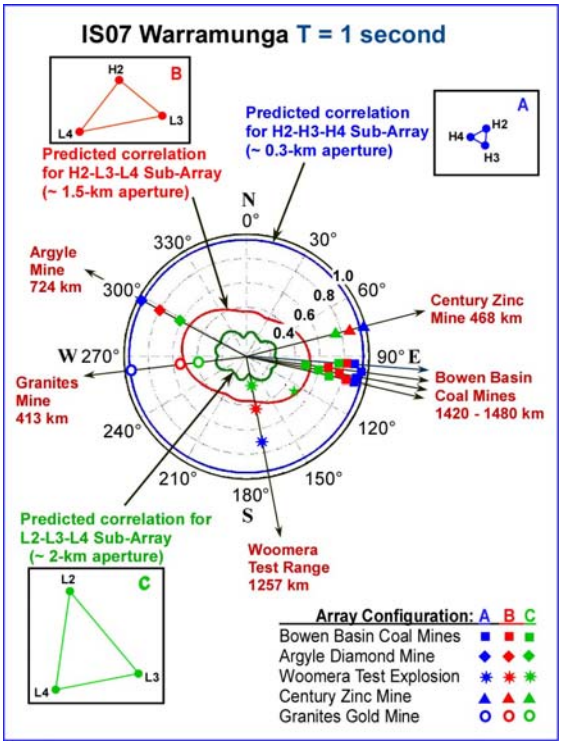


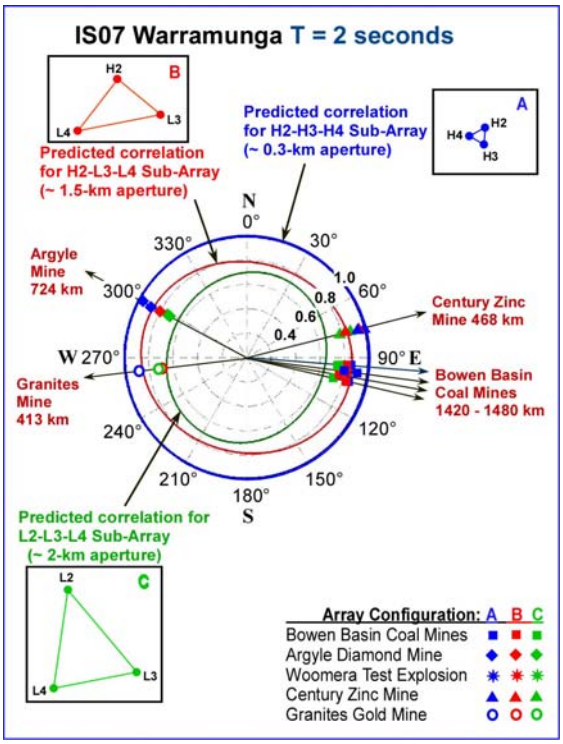


Figure 19b. Comparison of predicted and observed array-averaged correlation coefficients for 0.5 and 1.0 Hz infrasonic signals from regional and distant mining and chemical explosions recorded on small, medium and large aperture sub-arrays at IS07.

The results presented in Figures 18 and 19 show that the monitoring capability of triangular arrays with apertures of more than 2 km for small nuclear explosions will be, at best, marginal.

As part of this investigation of infrasound signal correlation properties, we have carried out a thorough survey of all detected explosion-generated events at certified IMS infrasound stations in Australia. An important result of this survey is the observation that the optimum passband for the detection of infrasound from regional and distant atmospheric explosions with yields of less than a few kilotons is restricted to a frequency range from about 0.4 to 1.2 Hz. The lower limit on this passband is determined by the presence of microbarom signals and the upper limit is set by the loss in signal correlation between array elements at higher frequencies. We will refer to this passband as the primary monitoring passband. The optimal detection passband for larger explosions may lie at frequencies below 0.1 Hz.

The predicted azimuthal distribution of the array-averaged correlation coefficient will now be used to determine the detection capability of 4-element rectangular and centered triangle infrasonic arrays, representative 8-element IMS arrays and 8- and 9-element pentagon arrays with triangular high-frequency sub-arrays.

The predicted azimuthal variation of the array-averaged correlation coefficient for a 1.5 km x 0.5 km rectangular array (Figure 20) provides a good example of an asymmetric sensitivity pattern at frequencies in the primary monitoring passband. The predicted correlation coefficient is also substantially attenuated at all azimuths at a frequency of 1.0 Hz. Spatial aliasing is a serious problem with 4-element array configurations of this type. The performance of rectangular arrays is very poor and they should not be used for explosion monitoring purposes.

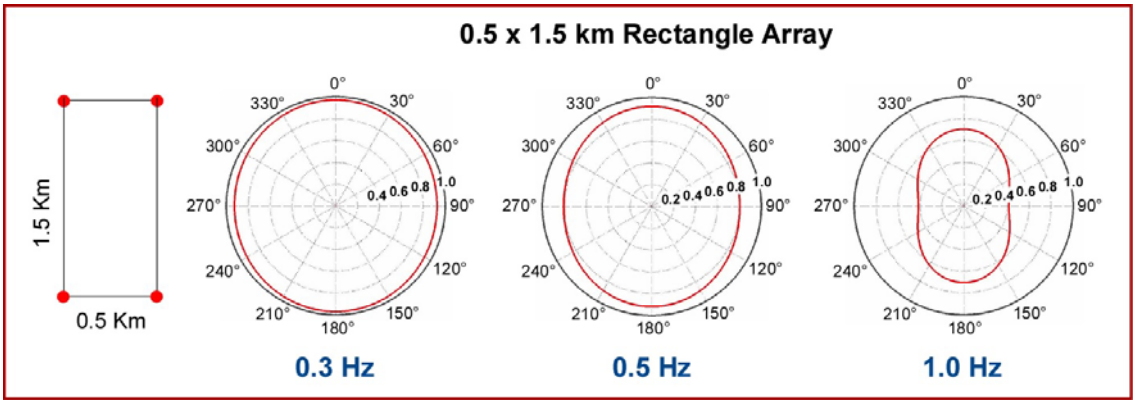


Figure 20. Azimuthal distributions of the array-averaged correlation coefficient predicted by the Mack and Flinn (1971) model for a 1.5 x 0.5 km rectangular array at frequencies of 0.3, 0.5 and 1.0 Hz. The correlation model parameters are $\Delta c = 15$ m/s and $\Delta\theta = 5°$ (Blandford, 1997).

A number of infrasonic arrays in the global monitoring network have been established as 4-element arrays with symmetrical centered triangle configurations. It is

well known that spatial aliasing of higher frequency signals is a potentially serious problem with these symmetrical 4-element arrays and existing arrays of this type in the IMS network are gradually being upgraded to 8-element arrays. We now examine the performance characteristics of centered triangle arrays from a signal correlation perspective. The calculated azimuthal distribution of the array-averaged correlation coefficient for centered triangle arrays with apertures of 1.0, 2.0 and 3.0 km are compared in Figure 21 for signals with frequencies of 0.5, 1.0 and 2.0 Hz.

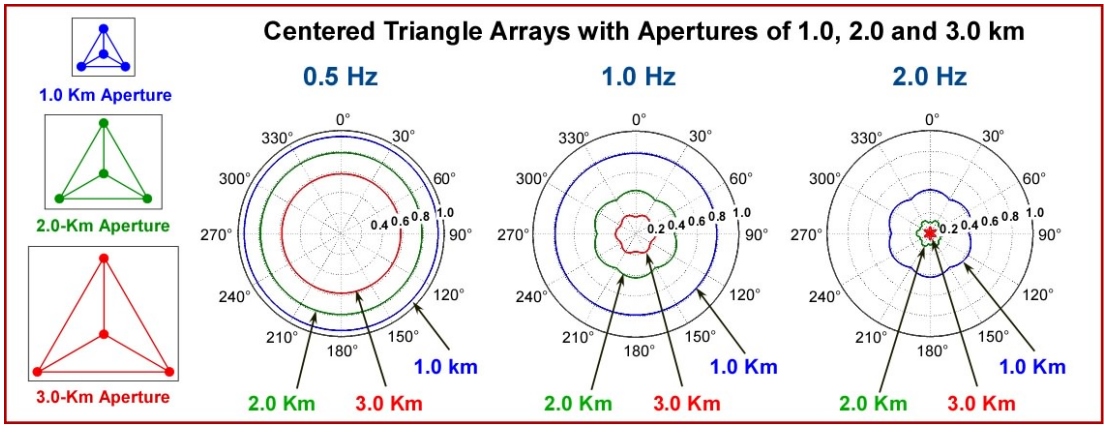


Figure 21. Azimuthal distributions of the array-averaged correlation coefficient predicted by the Mack and Flinn (1971) model for symmetrical centered triangle array configurations at frequencies of 0.5, 1.0 and 2.0 Hz. Results are shown in blue for a 1.0-km aperture array; in green for a 2.0-km aperture array and in red for a 3.0-km aperture array. The correlation model parameters are $\Delta c = 15$ m/s and $\Delta\theta = 5°$ (Blandford, 1997).

The predicted azimuthal array-averaged correlation patterns illustrated in Figure 21 for symmetrical centered triangle arrays are all reasonably isotropic. However, the predicted array-averaged correlation coefficient shows that there is a serious loss in signal correlation between array elements in most cases. The signal correlation results indicate that centered triangle arrays will have reasonable signal detection capability (ignoring the spatial aliasing problem) at a relatively low frequency of 0.5 Hz provided the array aperture is 2.0 km or less. The array correlation coefficient for 3.0-km arrays is significantly attenuated at 0.5 Hz. Detection capability for distant explosions will be reasonably good for 1.0-km aperture arrays, but very limited, at best, for 2.0- and 3.0-km aperture arrays at 1.0 Hz. The results presented for a frequency of 2.0 Hz show that signal correlation will be very small for all centered triangle arrays with apertures of 1.0 km or more at frequencies of 2.0 Hz or more. Higher frequency signals from distant explosions will not be detected reliably on centered triangle arrays with apertures of 1 km or more using automatic processing algorithms based on signal correlation

It might be expected that infrasound monitoring stations with 8 array elements arranged in a configuration with reasonable side-lobe suppression would have generally acceptable signal correlation properties. However, we have found that this is not necessarily true. This can be illustrated by the correlation properties for the three operational 8-element IMS infrasound monitoring stations, IS04, IS05 and IS07, located on the Australian continent. As can be seen from the array responses for each of these

stations (Figure 3), the array configurations at IS04, IS05 and IS07 exhibit fairly good side-lobe suppression. Each of these stations is configured in the form of a large aperture ("long-period") array with a small aperture ("high-frequency") sub-array. However, the array configurations at each of these stations differ substantially. The calculated polar distributions of the array-averaged correlation coefficients for the arrays at IS04, IS05 and IS07 are shown in Figure 22 for frequencies of 0.5, 1.0 and 2.0 Hz.

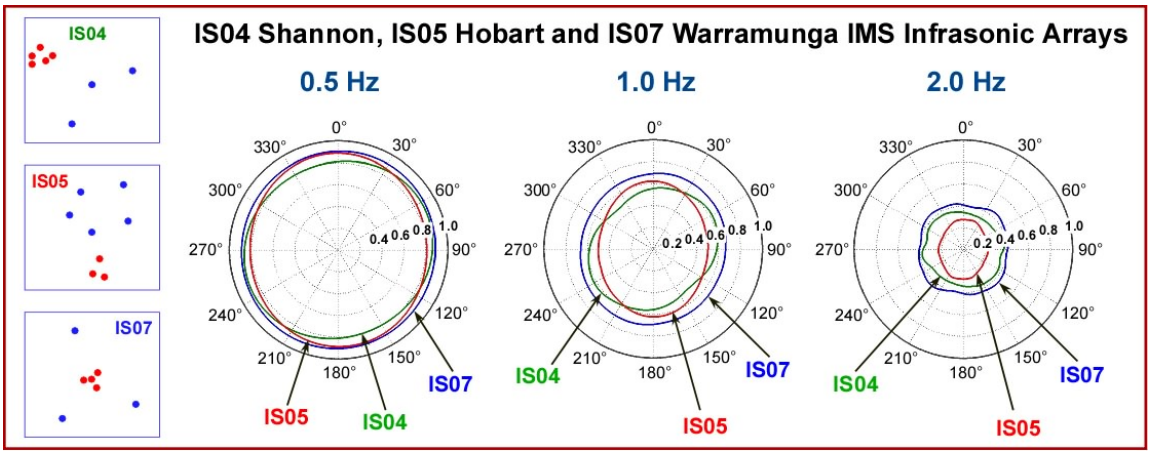


Figure 22. Azimuthal distributions of the predicted array-averaged correlation coefficient for 8-element IMS infrasound arrays at IS04, IS05 and IS07 at frequencies of 0.5, 1.0 and 2.0 Hz. The azimuthal variation of the array-averaged correlation coefficient is shown in green for the array at IS04; results in red correspond to the array at IS05 and results in blue correspond to the array at IS07. The array configurations are shown on the left hand side of the diagram. Calculations were carried out with $\Delta c = 15$ m/s and $\Delta\theta = 5°$.

As can be seen from Figure 22, the signal correlation properties of all arrays are fairly good at a frequency of 0.5 Hz, but the arrays at IS04 and IS05 exhibit some asymmetry in the azimuthal distribution of the array-averaged correlation coefficient. In addition, the array correlation in each case is attenuated, which reflects a loss in signal correlation between some site pairs in the array. The loss in signal correlation is much more pronounced at a frequency of 1.0 Hz. The polar distributions of the array-averaged correlation coefficient for IS04 and IS05 are also anisotropic at 1.0 Hz, which means that the sensitivity of these arrays is azimuthally dependent. The results for all arrays at a frequency of 2.0 Hz show that contributions to the array correlation coefficient are almost entirely due to site pairs in the high frequency sub-array. Thus, each of these arrays is reduced effectively to a small aperture sub-array at high frequencies. Detection at a frequency of 2.0 Hz is still possible at these arrays, but overall capability is reduced and the error on azimuthal measurement is increased. The array at IS07 with the small aperture sub-array embedded inside the main array has better performance characteristics than the arrays at IS04 and IS05. Small aperture "high-frequency" sub-arrays should not be located outside the main array configuration.

The procedures outlined above will now be used to determine optimal infrasonic arrays for monitoring regional and distant explosions. It is easy to design an optimal array with acceptable response and correlation characteristics when the number of array

elements is large. However, cost considerations in the IMS limit the number of array elements to a maximum of about 9. The search for an optimal array design will therefore be primarily concerned with 8- and 9-element arrays. We assume that the overall aperture of the array should be between 1.0 and 3.0 km and the array should be optimized for detection in the primary monitoring passband (0.4 to 1.2 Hz). The first step in this process is to determine a basic array configuration with an acceptable array response. This initial problem is essentially resolved for arrays with 8 or more array elements. Arrays with good side-lobe suppression can be designed using a larger aperture pentagon main array with an enclosed smaller aperture triangular sub-array, arrays in the form of a logarithmic spiral and arrays with randomly configured array elements. In recent years, there has been a tendency to install new 8-element arrays in the IMS in the form of a small aperture triangular array embedded inside a larger aperture pentagon array. We shall adopt this well-known basic configuration along with a similar 9-element configuration as basic designs for a suitable IMS infrasound monitoring array. The parameters that need to be optimized are the overall aperture of the main array and the size of the enclosed triangular sub-array. The array configuration and typical response of the 8- and 9-element pentagon arrays are illustrated in Figure 23. The response of each of these arrays is quite good. Both arrays have a few problematic side-lobes, but these can be effectively eliminated by using either (or both) slightly irregular central triangles or slightly irregular pentagons. The 9-element array is more robust than the 8-element array since the 9-element array will continue to have fairly good performance characteristics even when one of the array elements is down.

Examples of the predicted azimuthal variation of the array-averaged correlation coefficient for each of these basic array designs are presented in Figures 24 and 25 for overall array apertures of 1.0, 2.0 and 3.0 km, a triangular sub-array aperture of 0.3 km and frequencies of 0.5, 1.0 and 2.0 Hz. The results found for the 9-element array are only slightly better than the results found the 8-element array. In all cases, the azimuthal correlation patterns are nearly isotropic, even at high frequencies. However, in the case of the 2-and 3-km aperture arrays, the correlation coefficient at frequencies of 1.0 Hz or higher is attenuated and dominated by contributions from the small aperture triangular sub-array. In contrast, the 1.0 km aperture array has fairly good correlation characteristics even at a frequency of 2.0 Hz. We have examined the performance of each of these configurations for a wide range of sub-array apertures. The performance of the 8-element array deteriorates at higher frequency when the aperture of the central triangular sub-array exceeds about 250 m. The performance of the 9-element array at higher frequencies is largely independent of the size of the centered triangle sub-array up to an aperture of about 300 m. The size of the central sub-array should be chosen to be as large as possible in order to minimize the error on azimuthal measurements at high frequencies. Hence, we conclude that the optimal design parameters for pentagon arrays are:

a) 8-element array: 1 km overall aperture with a 0.25-km aperture triangular sub-array.

b) 9-element array: 1 km overall aperture with a 0.30-km aperture centered triangle sub-array.

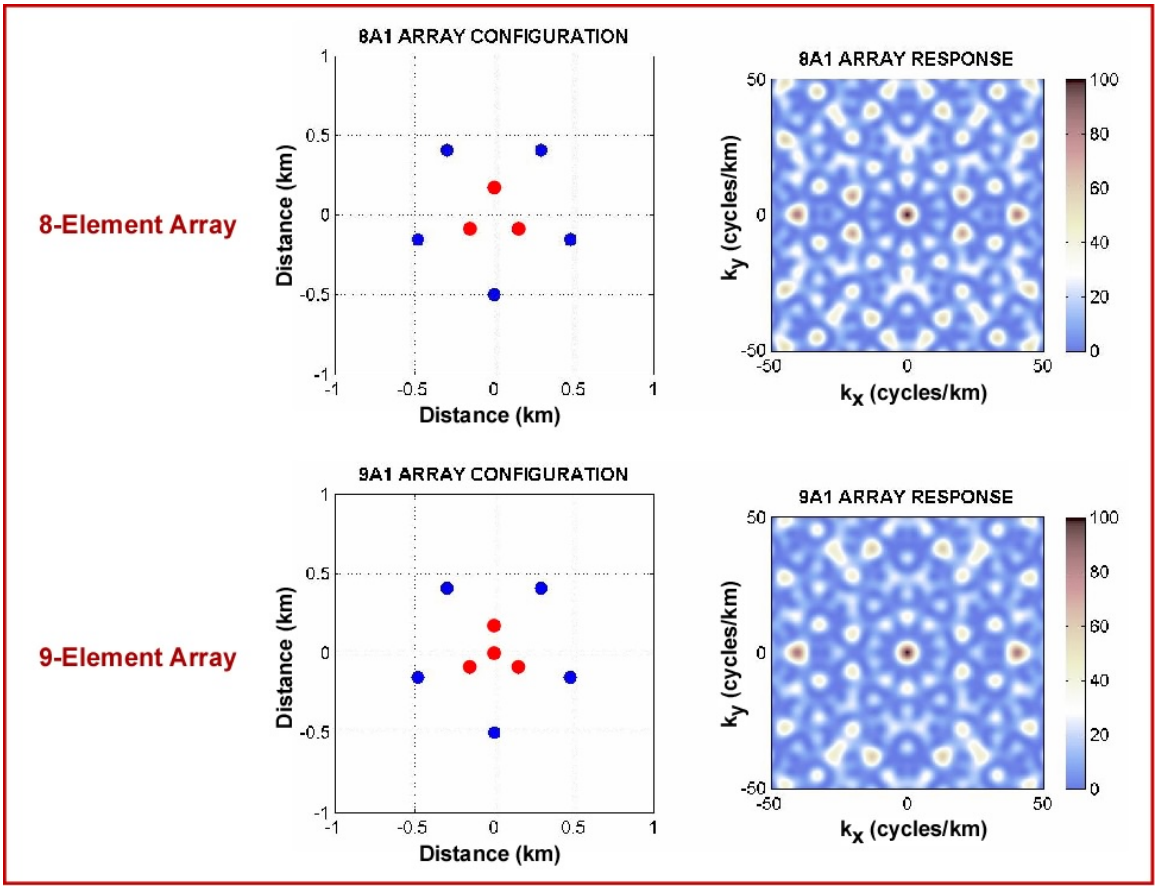


Figure 23. Array configuration and response of 8-element and 9-element pentagon arrays.

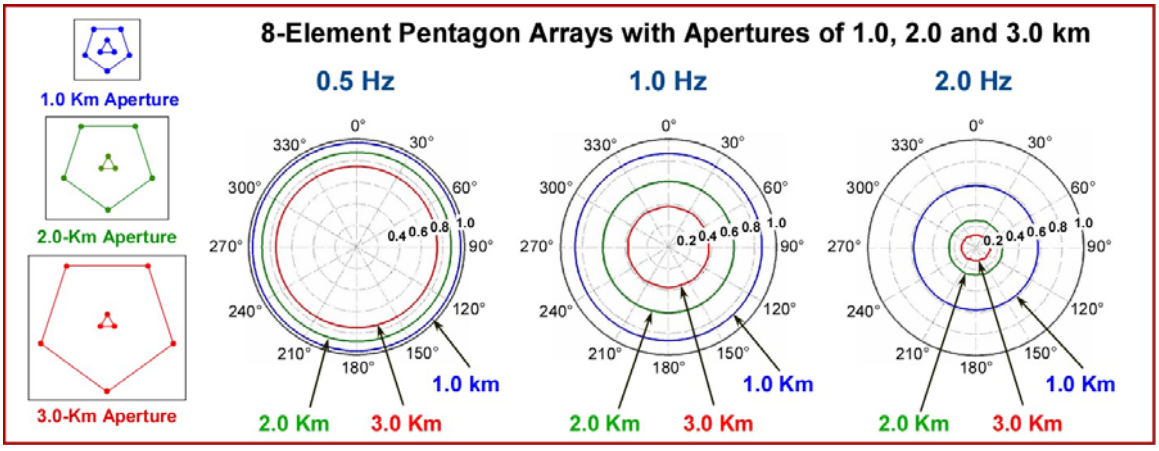


Figure 24. Azimuthal distributions of the array-averaged correlation coefficient predicted by the Mack and Flinn (1971) model for 8-element pentagon array configurations at frequencies of 0.5, 1.0 and 2.0 Hz. Results are shown in blue for a 1.0-km aperture array; in green for a 2.0-km aperture array and in red for a 3.0-km aperture array. The correlation model parameters are $\Delta c = 15$ m/s and $\Delta\theta = 5°$ (Blandford, 1997).

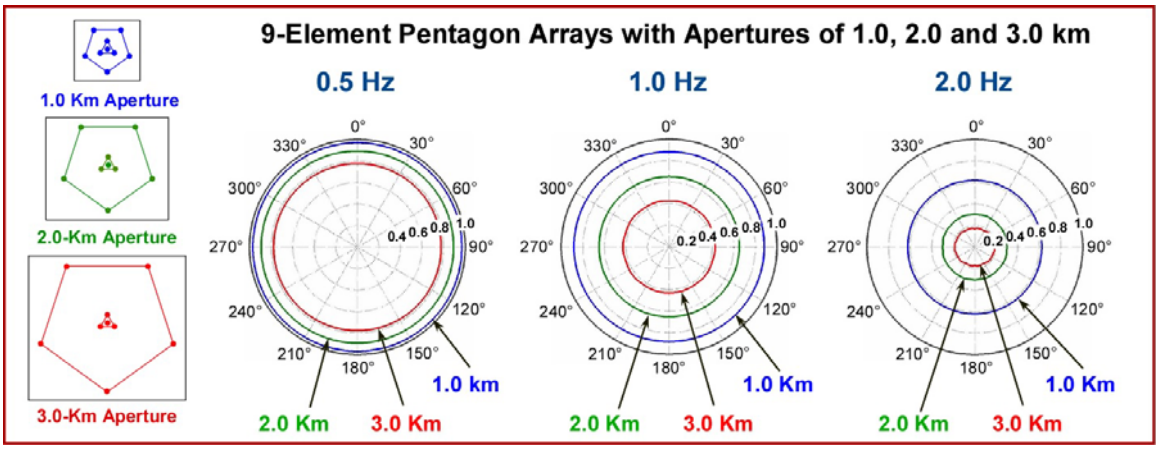


Figure 25. Azimuthal distributions of the array-averaged correlation coefficient predicted by the Mack and Flinn (1971) model for 9-element pentagon array configurations at frequencies of 0.5, 1.0 and 2.0 Hz. Results are shown in blue for a 1.0-km aperture array; in green for a 2.0-km aperture array and in red for a 3.0-km aperture array. The correlation model parameters are $\Delta c = 15$ m/s and $\Delta\theta = 5°$ (Blandford, 1997).

Other array configurations with at least 8 array elements can also be found with acceptable responses and good performance characteristics. Two possible examples are illustrated in Figure 26. In both cases, the optimal array design consists of a relatively small sub-array with an aperture of about 300 m enclosed inside a larger aperture array with an overall aperture of about 1 km. We recommend the use of the pentagon arrays described above for nuclear explosion monitoring purposes since these arrays have a well-defined geometry that can be easily implemented in the field.

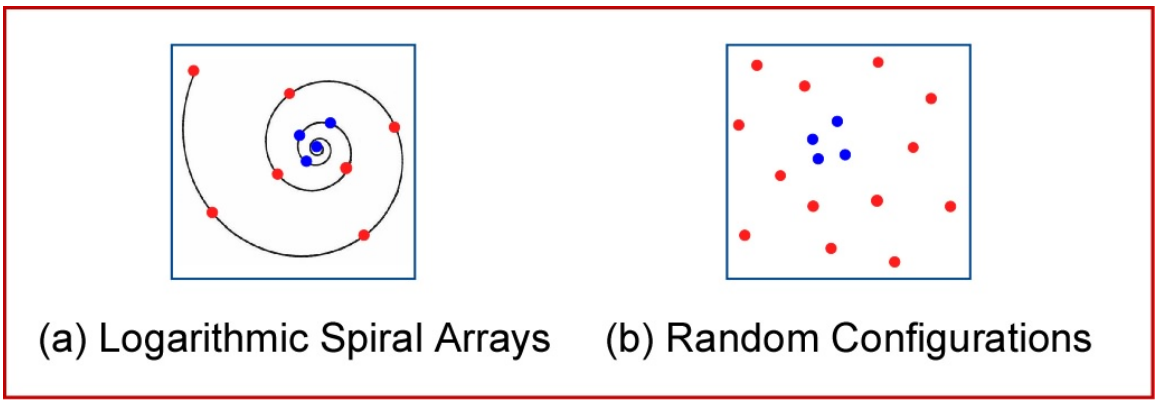


Figure 26. Typical examples of logarithmic spiral arrays and arrays with randomly configured elements.

As noted above, arrays with a large number of array elements can be designed with excellent performance characteristics. A few examples are illustrated in Figure 27. The 14-element array shown in (b) and the 19-element array shown in (d) in Figure 27 are particularly interesting since these arrays provide accurate measurements of signal azimuth at high frequency. This is accomplished by arranging the array elements in small

aperture clusters around the outer periphery of the array. The error on azimuthal measurements of signal azimuth at longer periods can also be reduced in arrays of this type by using an overall aperture that is larger than 1 km.

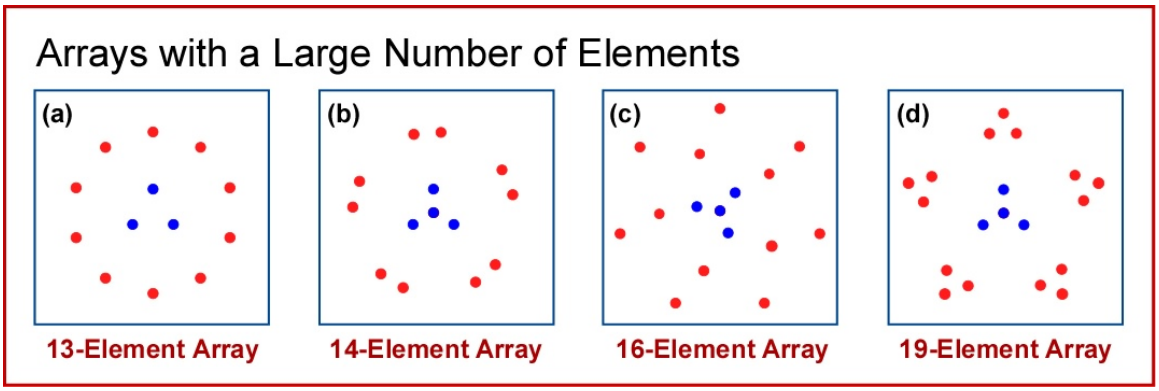


Figure 27. Typical examples of arrays with a large number of array elements.

In conclusion, the results presented in this Section show that the low degree of signal correlation between array elements in arrays with a small number of array elements may limit the reliable detection of regional and distant explosions at frequencies of 1.0 Hz and higher. These results also show that the optimum passband for the detection of infrasound from atmospheric explosions with yields of less than a few kilotons spans the frequency range from about 0.4 to 1.2 Hz. The study of the signal correlation properties of typical IMS arrays with a larger number of array elements shows that, even when an 8-element array has good side-lobe suppression characteristics, signal correlation between array elements may be reduced substantially and the sensitivity of these arrays may exhibit significant azimuthal anisotropy at higher frequencies. An investigation of the properties of 8- and 9-element pentagon arrays leads to the conclusion that arrays of this type have good performance characteristics when the overall aperture of the array is 1.0 km and the size of the inner triangular sub-array is set to an aperture of 0.25 km (8- element array) or 0.30 km (9-element array)

## 4.3. An Effective Wind-Noise-Reducing System

A number of different processes contribute to infrasonic background noise, including:

a) Wind-generated micropressure fluctuations associated with turbulent eddies in the atmospheric boundary layer;

b) Microbarom infrasonic waves in the 0.1 to 0.4 Hz passband;

c) Surf-generated infrasonic noise (usually at frequencies above 1.0 Hz);

d) Auroral-generated infrasound (usually at frequencies below 0.1 Hz);

e) Infrasonic noise generated by traffic, trains, aircraft, industry and other cultural sources (usually high frequency);

f) Various naturally occurring infrasonic sources such as on-going volcanic eruptions, forest fires, waterfalls etc.

g) Mountain-generated infrasonic waves (frequencies below 0.1 Hz);

h) Long-period micropressure fluctuations associated with slowly propagating gravity waves;

It is generally agreed that wind-generated noise is by far the most important source of infrasonic background noise. In this Section, we describe a new technique for wind-noise-reduction that has the potential to completely eliminate wind noise at infrasound monitoring stations.

Wind noise is a serious problem at most infrasound monitoring stations in the global network. At the present time, even with the use of current state-of-the-art wind-noise reduction systems, turbulent wind noise will prevent the detection of infrasonic signals from atmospheric explosions over significant periods of time if the array elements are exposed to the ambient winds. The problem is particularly serious at stations located on remote barren wind-swept islands and at stations located at high latitudes in the Arctic and Antarctic. Continental stations located in open fields or in semi-desert areas with sparse vegetation are also subject to high levels of wind noise, especially during the daytime. Noise levels at these stations may be much lower during the night when the upper level winds are decoupled from the surface by an intense nocturnal radiation inversion. Wind noise levels will usually be within acceptable limits at infrasound monitoring stations located in tall dense forests.

Typical background noise conditions at IMS infrasound monitoring stations can be illustrated by the noise conditions at the three operating infrasonic monitoring stations in Australia, IS04, IS05 and IS07. The environment and background noise conditions (see Figure 4) at each of these stations are described briefly in Section 3.1.1. IS04 Shannon is located in a very tall dense forest. Wind noise levels at this station are usually very low at all times of day and night. Thus, this well-sheltered station has exceptionally good detection capability in the primary monitoring passband. IS05 Hobart is located in a fairly sparse eucalyptus forest, which provides some shelter from the ambient winds. However, the forest has been cleared around the array elements and this results in rapidly changing wind-generated noise levels at most times of day and night which reduce the detection capability for atmospheric explosions. The diurnal variation and erratic behavior of the background noise at IS05 can be seen in the typical wideband array record section illustrated in Figure 28. IS07 at Warramunga is located in a semi-desert environment with little shelter from the ambient winds. Wind-generated noise levels are invariably high at this station under daytime convective conditions when the boundary-layer winds are coupled to the surface. The well-mixed boundary layer is replaced at night by a deep stable nocturnal radiation inversion, which effectively decouples the boundary layer winds from the surface and often results in very low noise conditions. The detection capability of this station is generally poor during the daytime, but may be exceptionally good at night. The diurnal behavior of the background noise levels at IS07 is illustrated in Figure 29. IS07 is also subject to sporadic nocturnal wind noise bursts associated with highly nonlinear mesoscale solitary waves and internal bore wave disturbances (Christie, 1989) that propagate on the nocturnal inversion layer. A variety of these unusual disturbances can be seen in the records shown in Figure 29.

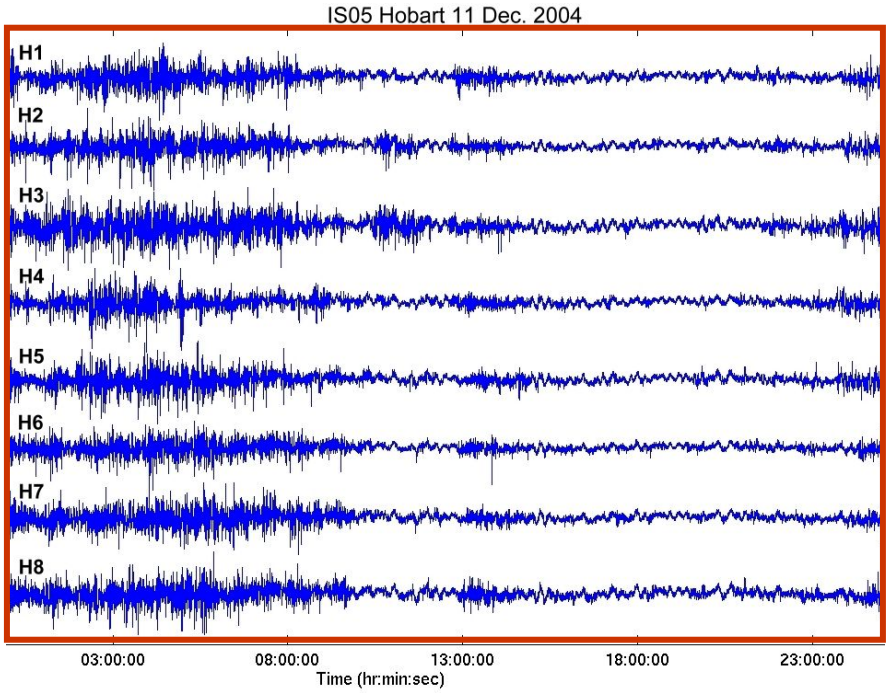


Figure 28. Typical wide-band micropressure signatures recorded at IS05 Hobart over a 24-hour period. Time is given in UT (LT = UT + 10:00).

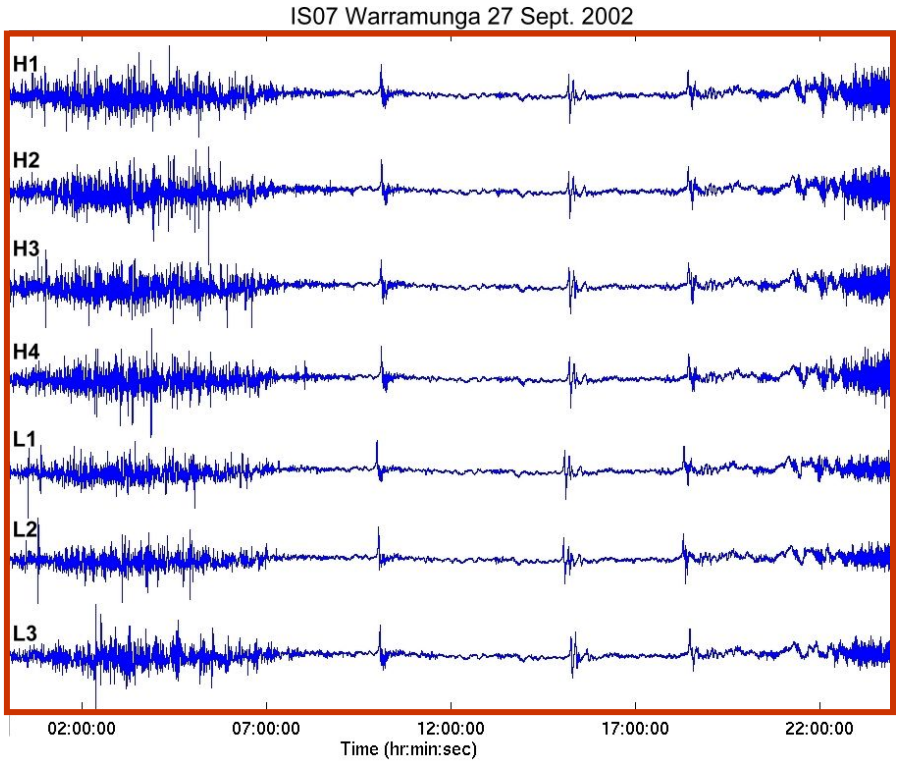


Figure 29. Typical wide-band micropressure signatures recorded at IS07 Warramunga over a 24-hour period. Time is given in UT (LT = UT + 09:30).

The investigation of signal correlation described in Section 4.2 has shown that the optimum passband for the detection of infrasound from regional and distant atmospheric explosions spans the frequency range from about 0.4 to 1.2 Hz. It is convenient to consider noise levels at a frequency of 1.0 Hz in order to discuss and assess the importance of wind noise on the detection capability of infrasound monitoring stations. Assuming that the signal-to-noise ratio for reliable detection of infrasound from regional and distant atmospheric nuclear explosions with a yield of 1 kiloton must be at least 1.0 or higher leads to the requirement that power spectral density estimates of background noise at 1.0 Hz must be less than about $0.5 \times 10^{-5}$ $Pa^2/Hz$. We note that this background noise level at monitoring stations equipped with the best conventional noise-reducing systems will be exceeded if the ambient winds (at a height of 2.0 m) are higher than about 2.5 m/s. We also note that average wind speeds during the daytime at typical unsheltered continental monitoring stations are usually in the range from about 2.5 to 4.0 m/s. These stations will therefore have poor detection capability during the daytime.

These remarks can be illustrated by the infrasonic background noise conditions at IS07 (see Figure 30). All of the IMS stations in Australia, including IS07, use DASE MB2000 infrasonic microbarometers with standard 18-m diameter, 96-port (or, in the case of the L-array sites at IS07, 70-m diameter, 144 port) CTBTO rosette noise-reducing pipe arrays (see Christie et al., 2001) on the input to the microbarometer. The lower limit on the noise at these stations in very low wind conditions is governed by the electronic noise floor of the MB2000 microbarometer ($\sim 4 \times 10^{-7}$ $Pa^2/Hz$ at high frequencies). This lower limit is clearly shown by the red curve corresponding to zero wind conditions in Figure 30. For comparison, we have also included the power spectral density estimates (blue curve) of background noise recorded simultaneously in zero wind conditions using a Chaparral Physics Model 5.1 microbarometer. This microbarometer has a much lower electronic noise floor than the MB2000 microbarometer and this is reflected in the significantly improved performance of the Chaparral Physics Model 5.1 sensor at all frequencies above 0.9 Hz. It is interesting to note that the high frequency observations given by the blue curve in Figure 30 of background noise under zero wind conditions appear to be the lowest observations made to date of background noise in the atmosphere at frequencies between 0.9 and 10 Hz. Thus the blue curve in Figure 30 provides a new low-noise model for infrasonic noise at frequencies above 0.9 Hz.

It is often stated that the noise floor of the MB2000 microbarometer does not present a limitation to the overall sensitivity of IMS infrasound monitoring stations since wind noise levels at most stations are almost always higher than this limit. We disagree with this statement for two reasons. The first is that even at existing IMS stations, noise levels at night under stable boundary layer conditions may be much lower than the noise floor of the MB2000 at higher frequencies. Secondly, the results presented below indicate that background wind noise can be essentially eliminated at most (if not all) infrasound monitoring stations. This means that the use of more sensitive infrasonic sensors can potentially improve detection capability at IMS stations.

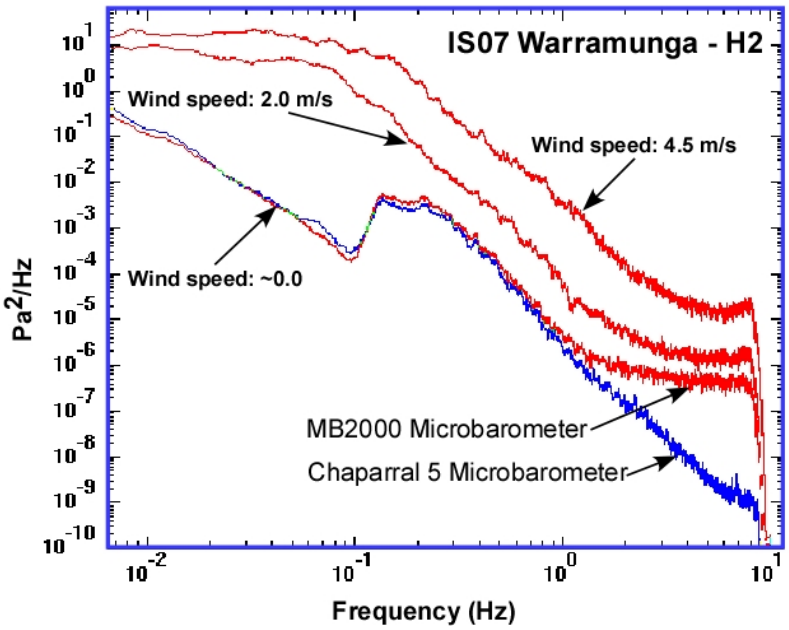


Figure 30. Power spectral density of infrasonic background noise recorded at site H2 at IS07 Warramunga. Curves shown in red correspond to the DASE MB2000 microbarometer used with a standard 18-m diameter rosette noise-reducing system on the input to the microbarometer. The blue curve corresponds to data recorded in zero wind using a Chaparral Physics Model 5.1 microbarometer.

The observations presented in Figure 24 show that the average noise levels at 1 Hz at IS07 range from about $2 \times 10^{-6}$ $Pa^2$/Hz at night in very low wind conditions to about $3 \times 10^{-3}$ $Pa^2$/Hz during the daytime. Since noise levels at 1.0 Hz should be less than $5 \times 10^{-5}$ $Pa^2$/Hz in order to meet essential monitoring requirements, the 1.0 Hz noise levels at typical unsheltered continental IMS infrasound stations equipped with conventional wind-noise-reducing pipe arrays need to be further reduced by at least two orders of magnitude.

Most of the methods that have been used in the past to reduce wind noise have been based on a spatial averaging of the micropressure field over a limited area surrounding the array element location using pipe arrays with a large number of discrete inlet ports or pipe arrays constructed from sections of porous hose (see, e.g., Alcoverro, 1998; Christie et al., 2001; Christie, 2002; Hedlin et al., 2003, Alcoverro and Le Pichon, 2004). Examples of the pipe arrays that have been designed for use in the IMS infrasound network are shown in Figure 31. Effective noise reduction has also been achieved (Zumberge et al., 2003, Walker et al., 2007) using a distributed optical fiber infrasound sensor (OFIS) to average pressure fluctuations along a line.

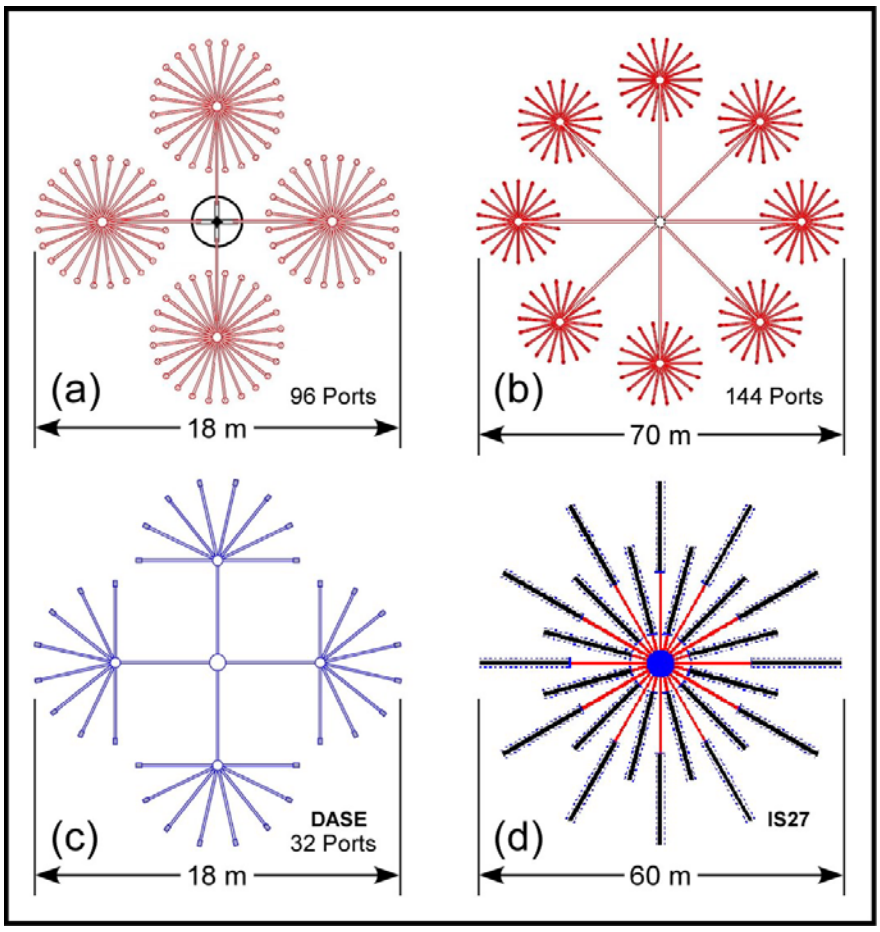


Figure 31. Wind-noise-reducing pipe arrays used at stations in the IMS infrasound network. The 18-m diameter rosette design shown in (a) is installed at all sites in IS04 and IS05 and also at the H-sites at IS07. The 70-m diameter rosette design shown in (b) is installed at the L sites at IS07. The rosette pipe array designs shown in (a) and (b) (Christie et al. 2001) are used at many other IMS infrasound stations. The design illustrated in (c) (Alcoverro, 1998) is also used at a large number of IMS infrasound stations. The specialized design illustrated in (d) (Christie, 2002) is used at IS27 Neumayer Base in Antarctica. This pipe array is constructed from sections of porous hose enclosed in perforated pipes and is designed to operate under snow cover in Arctic and Antarctic conditions.

Almost every conceivable wind-noise-reducing pipe array design has been tested during the last 40 years (Christie, 2006). It seems very unlikely that further refinements to pipe array designs will lead to significant improvements in performance since the size of the area that can be used and the number of inlet ports have reached practical limits. The use of compact arrays consisting of a large number of individual sensors and digitizers combined with adaptive signal processing has been proposed as an enhanced noise-reducing technique (Tamadgee et al. 2001; Bass and Shields, 2004, Shields, 2005). This procedure will undoubtedly provide some improvement, but it seems unlikely that noise levels can be reduced by more than two orders of magnitude over that which is provided by existing wind-noise-reducing systems. Wind barriers based on the original design

pioneered by L. Liszka at the Swedish Institute of Space Physics in 1972 have also been used to reduce wind noise and enhance signal-to-noise ratios (ReVelle, 1998; ReVelle, private communication, 2000; Hedlin and Berger, 2002, Hedlin and Raspet, 2003). These noise-reducing systems are effective at higher frequencies, but provide little improvement at frequencies in the primary monitoring passband. Finally we note the important work of Bedard et al. (2003) who successfully used a porous wind fence with corrugations to reduce wind noise during an investigation of higher frequency infrasound generated by tornadoes.

It seems clear that a new approach is required to resolve the wind-noise problem at infrasound monitoring stations (Christie, 2007). New and effective techniques have therefore been developed that essentially eliminate the wind-noise problem. These techniques are based on:

a) The lifting of the turbulent boundary layer above the sensor inlet or inlets,

b) The transformation of wind-generated turbulent eddies into smaller scale eddies that produce micropressure fluctuations that lie outside the monitoring passband, and

c) The extraction of energy from turbulent eddies at all frequencies in the monitoring passband.

All tests on the development of new wind-noise-reducing systems have been carried out at IS07 Warramunga located in the arid interior of the Northern Territory of Australia. As noted above, IMS infrasound station IS07 is invariably subject to unacceptably high levels of wind-generated noise during the daytime with average daytime wind speeds in the range from about 2.7 to 4 m/s (as measured at a height of 2.0 m). The wind noise conditions encountered at Warramunga are typical of wind noise conditions found at many IMS infrasound stations. The primary goal of this project is to develop a wind-noise-reducing system which will effectively reduce wind noise to acceptable levels at all times of day or night at infrasound monitoring stations, such as Warramunga, that are located in areas with little shelter from the ambient winds. We anticipate that the techniques that are developed for use at Warramunga can also be adapted for use at stations located in higher wind environments. It is clear that the development of a wind-noise-reducing system that is capable of reducing wind noise at IS07 Warramunga to acceptable levels in the monitoring passband has the potential to resolve wind-noise problems at more than 90% of all IMS infrasound monitoring stations.

The first attempt to develop an improved wind-noise reducing system was based on the use of surface screens, which lift the turbulent boundary layer over the inlets in a conventional pipe array system. This system (see Figure 32) eliminates any unwanted dynamic pressure contributions and may reduce the influence of daytime convection. The system effectively improves noise reduction at a frequency of 1 Hz by a factor of about 3 in winds of 3.5 m/s, which is probably more than the reduction that could be achieved by any refinement to existing pipe array designs. However, the reduction in wind noise is much less that that required for reliable signal detection at stations located in high wind environments.

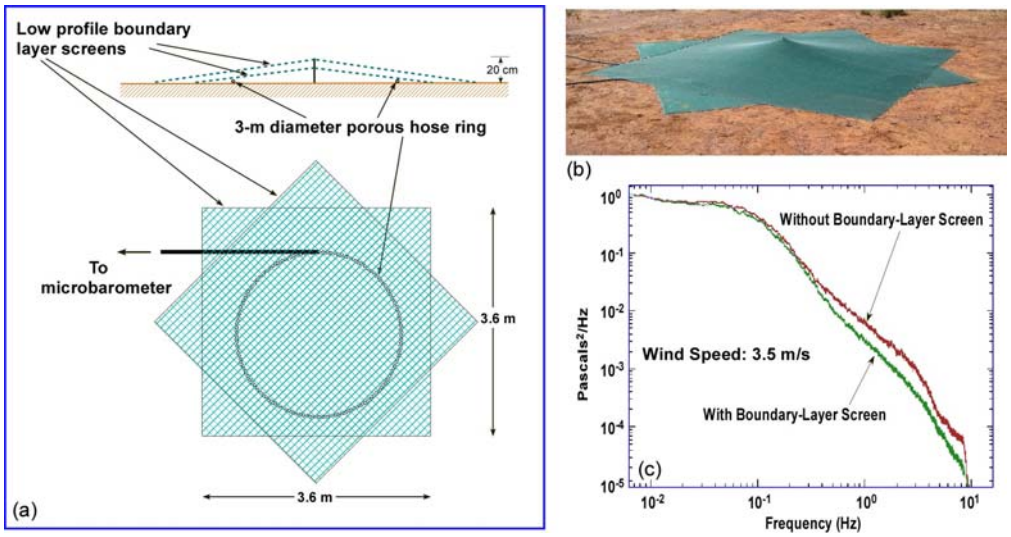


Figure 32. Wind-noise-reducing surface screen.

### 4.3.1 Turbulence-Reducing Enclosures

It was decided at this point that it might be possible to develop an effective wind-noise-reducing system by using a screened enclosure with multiple walls to remove energy from turbulent eddies in the atmospheric boundary layer. Two versions (Versions 1 and 2) of a turbulence-reducing enclosure were constructed and tested. These initial designs are illustrated schematically in Figure 33. The design of these enclosures is based on the following criteria:

a) The interaction of the enclosure with the ambient flow should not create unwanted turbulence. This can be achieved by using porous walls, which allow part of the ambient wind to flow through the structure. We have used screening materials with porosities between 30 and 50 % without any problems. The precise value of the porosity does not appear to be important. However, solid walls must not be used since this will generate unwanted turbulence and may attenuate signals.

b) The top of any porous wall in the structure should not be horizontal since the flow will fold over this boundary normal to the edge and create turbulence at lower levels behind the boundary. Bedard et al. (2003) used solid vertical corrugations along the upper edge of their wind fence in an attempt to avoid this problem. Here, we use a modified version of this technique, which should be more effective. The porous walls in the enclosures illustrated in Figure 33 are constructed with deep porous serrations along the top edge. The ambient turbulent flow will fold normally over the edge of each of these serrations and the residual flow will tend to cancel on the back side of the serrations. Note that the deep serrations in this case are inclined away from the center of the enclosure (see the cross section of the walls in Figure 33). This is done for the following reason. If the serrations are vertical or inclined towards the center of the enclosure, the normal flow over the edge of the serrations will have a downward component. Any residual turbulence that is left behind the serrations will then be mixed to lower levels in the interior of the enclosure. On the other hand, if

the serrations are inclined away from the center of the enclosure, the residual disturbances behind the serrations will have an upwards component which will hopefully carry the residual turbulent eddies into the undisturbed flow aloft that is sweeping over the structure. We have also incorporated a noise-reducing surface screen into the design of these turbulence-reducing enclosures.

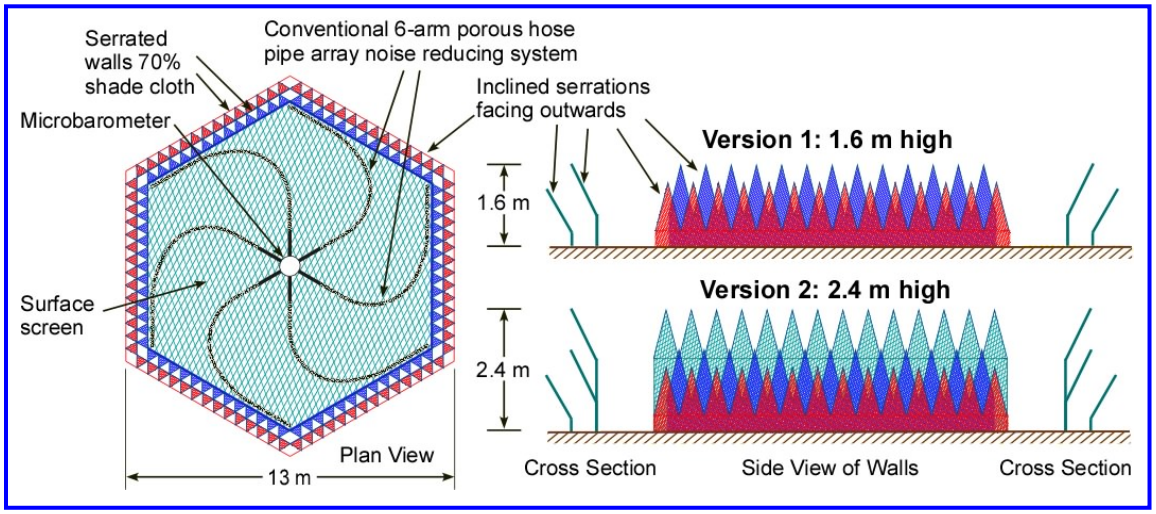


Figure 33. Schematic diagram illustrating two versions of a turbulence-reducing enclosure combined with a surface noise-reducing screen. Version 1 of the enclosure is 1.6 m high with two porous walls with overlapping deep serrations inclined away from the center of the enclosure. Version 2 of this system is 2.4 m high with 3 rows of inclined overlapping deep serrations arranged on two porous walls. The plan view shows the layout of the conventional 6-arm porous hose pipe array system, which was used to evaluate the performance of these noise-reducing systems.

These wind-noise-reducing systems were evaluated by simultaneously comparing measured background noise data recorded using a conventional 6-arm porous hose noise-reducing pipe array located on the surface inside the enclosure with data recorded simultaneously using an identical porous hose pipe array located in an open area near the enclosure.

The performance of the 1.6-m high turbulence reducing enclosure with two rows of serrations is summarized in Figure 34. As can be seen from the results shown in this diagram, the 1.6-m high turbulence-reducing enclosure provides a significant reduction in wind noise in low and moderate winds. However, the efficiency decreases rapidly when wind speeds exceed 3.2 m/s. Furthermore, while the degree of wind-noise reduction in modest winds is significant (a little over 1 order of magnitude in winds of 3.2 m/s), the performance of this enclosure does not meet the necessary requirements for wind noise reduction at stations located in high wind environments. The results show that the performance of this enclosure might be good enough for infrasound stations that are located in sparse forests or other partially sheltered environments where the ambient winds are less than 2.5 m/s.

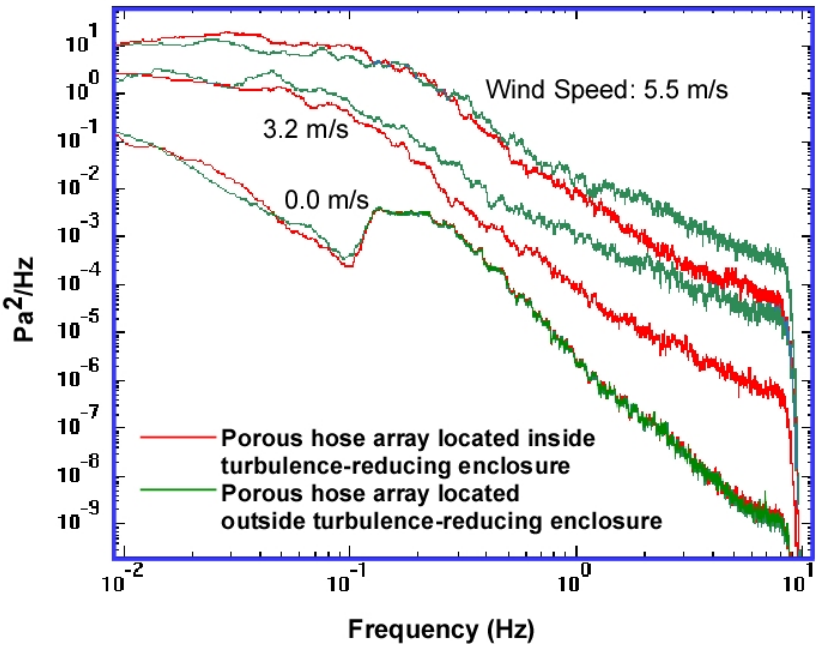


Figure 34. Power spectral density of background noise recorded using a conventional porous hose pipe array system located inside Version 1 of the enclosure with 1.6-m high walls (red curves) compared with the power spectral density of background noise recorded simultaneously on an identical pipe array system located outside the enclosure (green curves) for wind speeds (at a height of 2.0 m) of 0.0, 3.2 and 5.5 m/s.

In view of the relatively limited performance of the 1.6-m high enclosure, we decided to enhance this design by increasing the height of the enclosure to 2.4 m and adding a further row of overlapping serrations. These changes resulted in a significant improvement in the performance of this structure. An example of noise suppression in the frequency range from 0.4 to 6.0 Hz provided by Version 2 of the enclosure is shown by the waveform data presented in Figure 35.

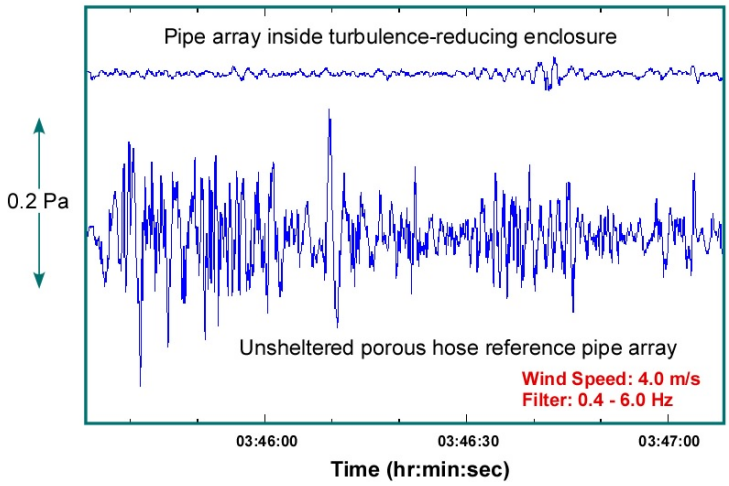


Figure 35. Waveform data showing the large reduction in background noise in the frequency range from 0.4 to 6 Hz provided by the 2.4-m high turbulence-reducing enclosure (Version 2) for a wind speed of 4.0 m/s.

A summary of the performance of Version 2 of the enclosure in winds of up to 6.0 m/s is presented in Figure 36. As can be seen from these results, background noise reduction in the monitoring passband is enhanced considerably when a conventional pipe array system is placed inside the turbulence-reducing enclosure, especially when the ambient winds are less than about 4 m/s. Indeed, these results suggest that the use of this type of turbulence-reducing device in conjunction with a conventional pipe array system will reduce the degree of wind noise in the primary monitoring passband to acceptable levels for nuclear explosion monitoring when the ambient winds are less than about 4 m/s. To be more specific, the results in Figure 36 show that background wind noise levels are reduced by more than two orders of magnitude at 1.0 Hz in winds of up to 4.5 m/s over the level of noise reduction obtained by a conventional noise-reducing pipe array alone. We also note that the noise level obtained using this turbulence-reducing enclosure in conjunction with a conventional noise-reducing pipe array in a wind speed of 4.5 m/s is less than $5 \times 10^{-5}$ $Pa^2/Hz$, even though the conventional noise-reducing system used to evaluate this system is of smaller diameter and less efficient than the 18-m diameter rosette noise reducing pipe arrays used at most existing IMS stations. Since many IMS monitoring stations are subject to average wind speeds of up to about 4 m/s, the use of noise-reducing enclosures of this type in conjunction with existing pipe arrays can potentially resolve wind noise problems at these stations.

However, while the results presented in Figure 36 show that the enclosure continues to provide enhanced noise reduction as the winds increase above 4 m/s, the results also show that the performance of the system will not be good enough to ensure the reliable detection of signals from distant explosions when the system is used in high wind environments. As with Version 1, the efficiency of Version 2 of the system also decreases in higher ambient winds starting at about 4.5 m/s. There is still some noise reduction at 1.0 Hz in ambient winds of 6.0 m/s, but this amounts to only about a factor of about four and does not reach the requirements for reliable nuclear explosion monitoring. The results suggest that Version 2 of the turbulence-reducing enclosure will have virtually no noise-reducing capability in the primary monitoring passband when the ambient winds exceed about 7 m/s. We therefore conclude that Version 2 of the wind-noise-reducing system will not be useful at nuclear explosion monitoring stations that are subject to sustained winds of greater than about 5 m/s. Again, however, we note that the use of Version 2 of the system in conjunction with a conventional pipe array can potentially resolve wind-noise problems at about 90% of the monitoring stations in the IMS.

The comparison of the performance of Version 1 (1.6-m high) and Version 2 (2.4-m high) suggests that an increase in the height of the enclosure is beneficial. We therefore increased the height of the enclosure to 3.2 m in an attempt to improve performance in high winds. The inner wall in this design (Version 3) was increased to a height of 3.2 m with a third row of inclined serrations along the top edge. We also changed the design of the "conventional" porous hose pipe array systems in an attempt to enhance performance at longer periods. In the original spiral array configuration, the porous hoses were connected to the microbarometer using a 2-m section of impervious hose. The length of the impervious hose section on each arm was increased to 5 m so that most of the porous hose occupies the outer perimeter of the available area inside the enclosure.

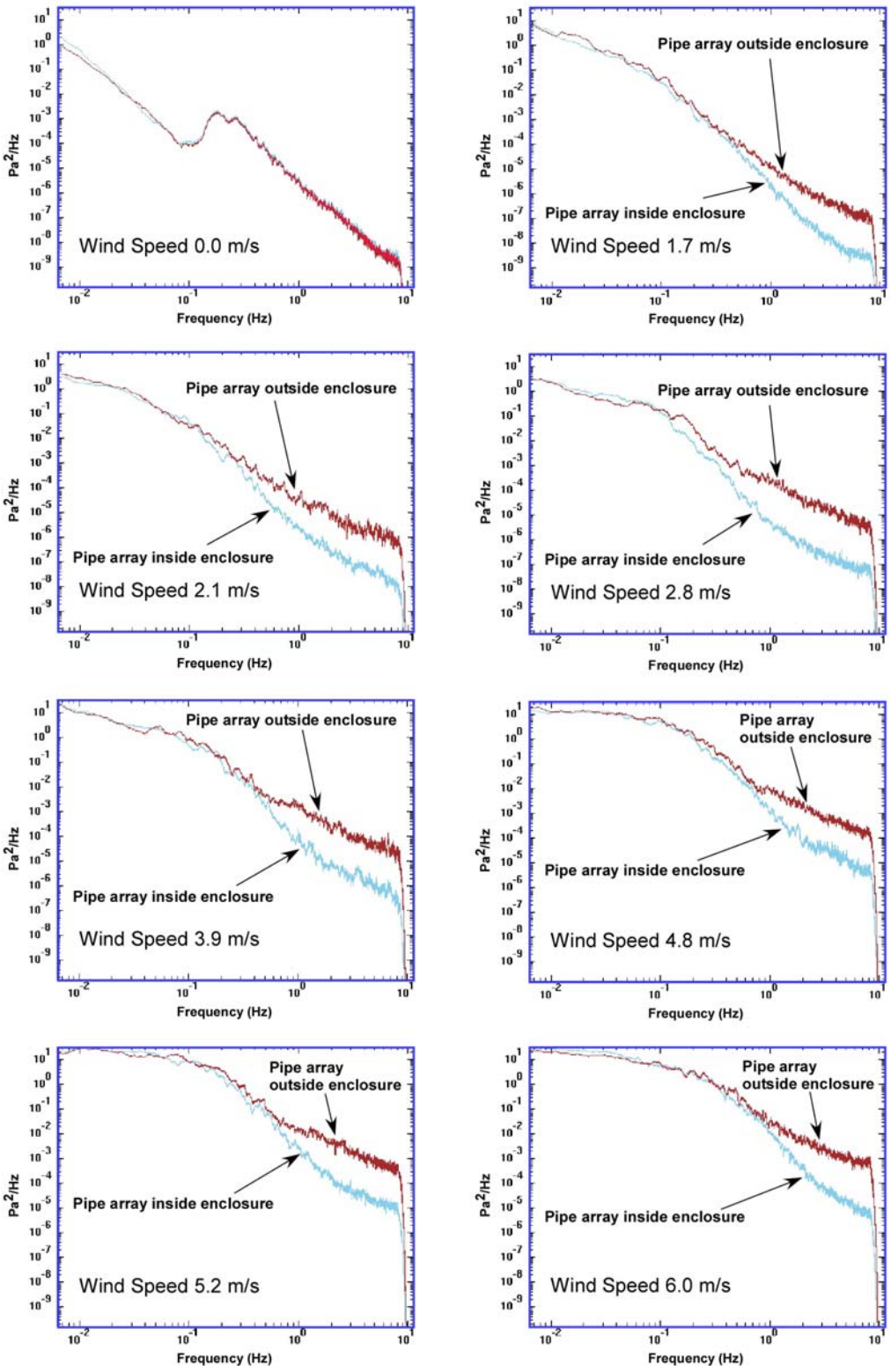


Figure 36. Comparison of power spectral density of infrasonic background noise for conventional pipe array systems located inside and outside the 2.4-m high (Version 2) turbulence-reducing enclosure for wind speeds up to 6.0 m/s

Version 3 of the enclosure was tested for only a short period of time. Since flow through the walls at higher levels below 3.2 m was judged to be turbulent, Version 4 of the enclosure was constructed by including a new outer 3.2-m high wall. Schematic illustrations of Versions 3 and 4 of the turbulence-reducing enclosure are shown in Figure 37.

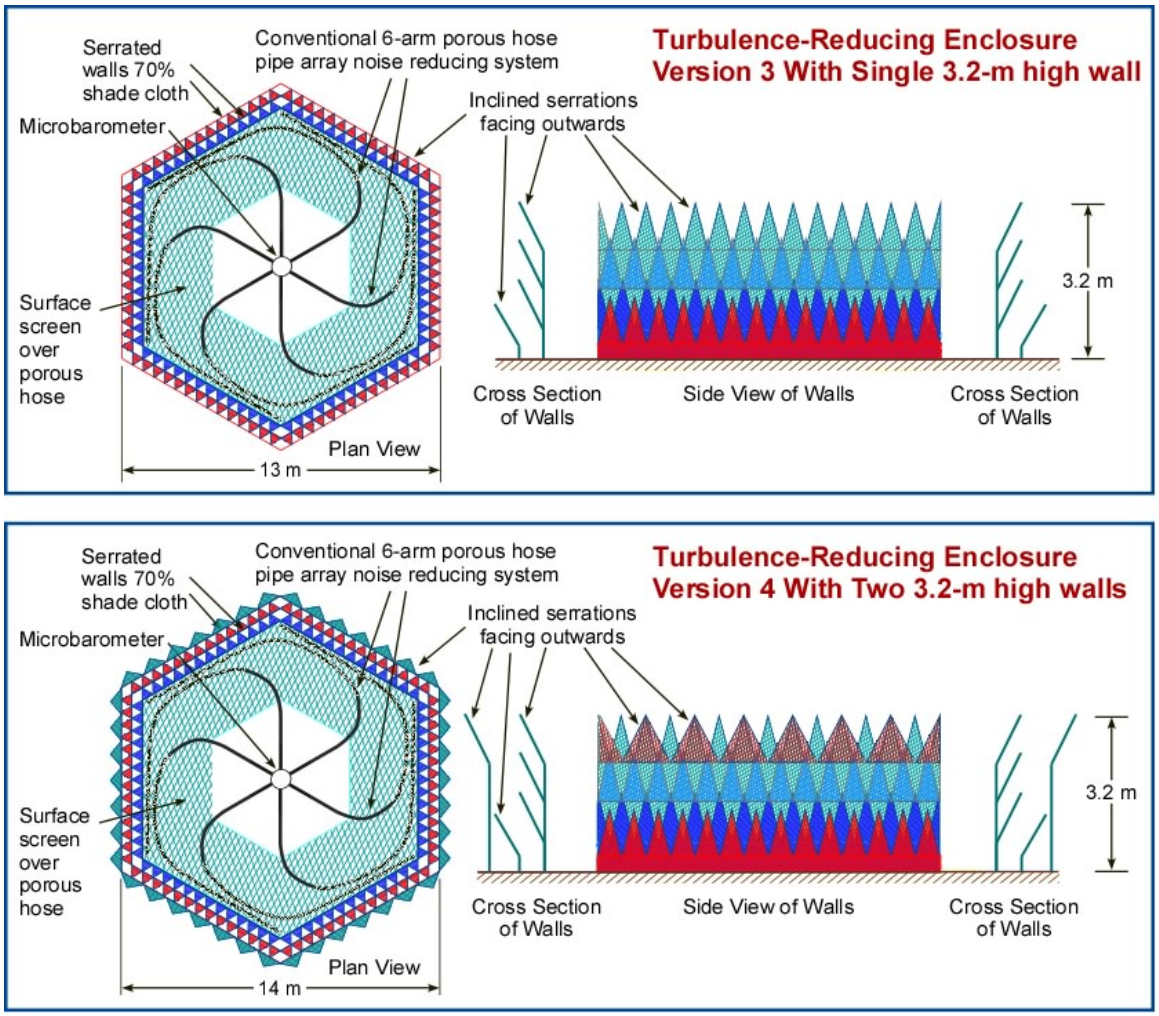


Figure 37. Schematic diagram illustrating the design of Versions 3 and 4 of the turbulence-reducing enclosure. The inside wall in Version 3 has been extended to a height of 3.2-m with an additional row of deep overlapping inclined serrations along the top edge. Version 4 has a new outer 3.2-m high outer wall with larger outward facing inclined serrations along the top.

Version 4 of the enclosure was tested at IS07 in ambient winds of up to about 5.8 m/s. Some serious difficulties were encountered with the "conventional" porous hose pipe arrays that were being used to evaluate the performance of the new enclosure system after the onset of monsoonal storms in northern Australia during the test period. In particular, we found that these conventional pipe array systems fail to work reliably once they become saturated by heavy rain and covered with silt-laden ground water. In order to

avoid these problems, we replaced the porous hose pipe array systems inside and outside the enclosure with more robust 6-port pipe array systems. The performance of Version 4 of the noise reducing enclosure with 3.2-m high walls was found to be virtually the same as the performance of Version 2 of the enclosure with 2.4 m high walls at 1.0 Hz in ambient winds of up to about 4.5 m/s. The performance of this enclosure at 1.0 Hz is marginally better than Version 2 at wind speeds above 4.5 m, but, again, the performance starts to deteriorate in higher winds when ambient winds exceed about 5.5 m/s.

It would appear that there is little point in increasing the height of the walls in these enclosures beyond 3.2 m. The ambient boundary layer winds increase fairly rapidly with height above the surface. An examination of the flow inside the enclosure showed that the upper serrations on the top of the 3.2-m walls are interacting with the higher winds at this height and this in turn has resulted in further unwanted turbulence that is being mixed to lower levels inside the enclosure. This effect was manifested in higher ambient winds as a fairly low intensity induced irregular turbulent flow that circulates around the inside of the enclosure.

At this point we decided: a) to examine the micropressure noise field in more detail inside the enclosure, b) to devise techniques that will eliminate induced flows and turbulence inside the enclosure and c) to examine the merits of using only a single inlet port system inside the turbulence reducing enclosure.

The noise survey inside the enclosure showed that the maximum noise levels at 1.0 Hz occur at the midway point between the center and the inner walls of the structure. They also showed that noise levels in the corners of the hexagonal structure (see Figure 37) at the wall are significantly lower than the noise levels at any other point in the enclosure. These observations provide the basis for using a simple 6-port pipe array system with the inlet ports located in the vertices of the hexagonal structure.

As a first attempt to further reduce turbulence inside Version 4 of the enclosure, we constructed an inner chamber with 1.8-m high screened walls surrounding a single inlet port system located near the center of the enclosure. The damping of the turbulent flow inside the structure due to these interior walls resulted in only a minor improvement in observed noise levels on both the single inlet port system and the pipe array system. We then introduced a series of twelve 2.0-m high symmetrically positioned radial baffles inside the structure to reduce the induced turbulent circulations in the interior of the enclosure. As can be seen from the results shown in Figure 38, the radial baffles improve background noise reduction at all frequencies above about 0.1 Hz. These baffles are, however, more effective at higher frequencies.

We were somewhat surprised to find that the noise levels recorded on the single inlet port system located near the center of the enclosure are only slightly reduced when this port is surrounded by a small open enclosure with 1.8-m high screened walls. We therefore decided to isolate this single port system by installing a screened roof over the inner structure. As shown by the results presented in Figure 39, the addition of a screened roof to the inner structure resulted in a significant improvement in the performance of the single inlet port system, especially at higher frequencies.

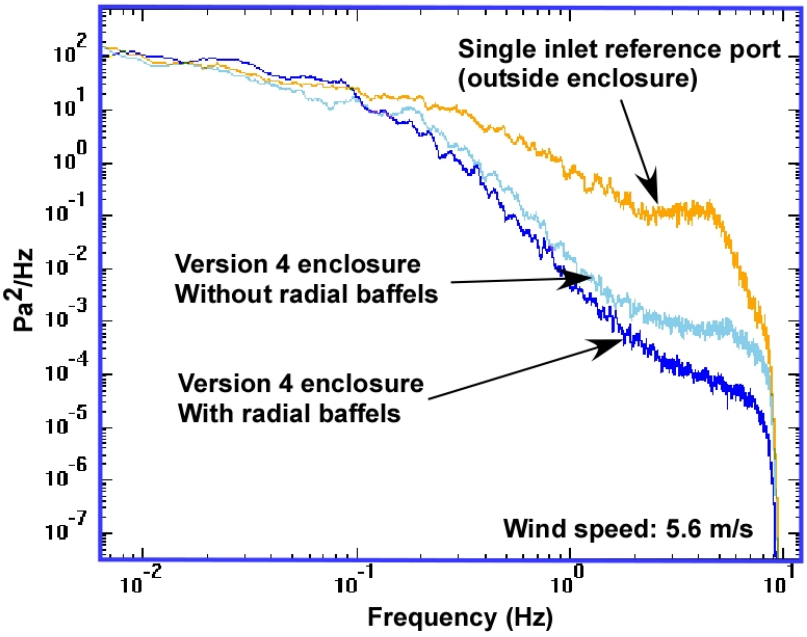


Figure 38. Comparison of power spectral density estimates of infrasonic data recorded with a conventional pipe array located inside Version 4A of the turbulence reducing enclosure before (light blue curve) and after (dark blue curve) the installation of 12 radial vertical baffles. The average wind speed at the time of these measurements was 5.6 m/s.

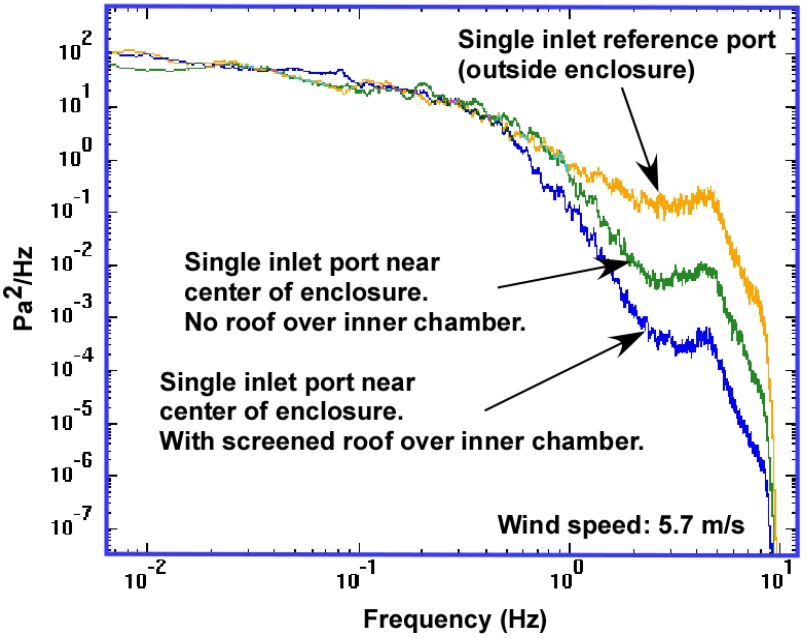


Figure 39. Comparison of power spectral density estimates of infrasonic data showing the influence on background noise levels of a screened roof over the inner chamber surrounding a single inlet port system located near the center of Version 4A of the turbulence-reducing enclosure.

We shall refer to the version of the open enclosure with the changes described above a Version 4A. This version was tested under a wide range of wind conditions over a period of about 4 weeks. The results of these tests showed that the single centrally located inlet port system is surprising effective and may even perform better than a conventional pipe array at high frequencies. This can be attributed to the turbulence-reducing influence of the closed inner chamber that surrounds this single inlet port.

The results shown in Figure 38 show that the construction of a screened roof over the inner chamber resulted in a fairly substantial reduction in background noise levels. We therefore decided to install a screened roof over the entire interior of the enclosure at a height of 2.0 m above the surface. The installation of this roof removed almost all traces of the low intensity induced swirling flow inside the enclosure, even in the highest ambient winds. We also decided to further isolate the central inlet port with a second smaller enclosure located inside the inner chamber in hopes that this might improve the performance of a single-port system. All of these changes, including the 6-port hexagonal pipe array, are shown in the schematic diagram of the enclosure presented in Figure 40. This version of the turbulence-reducing enclosure will be referred to as Version 4B.

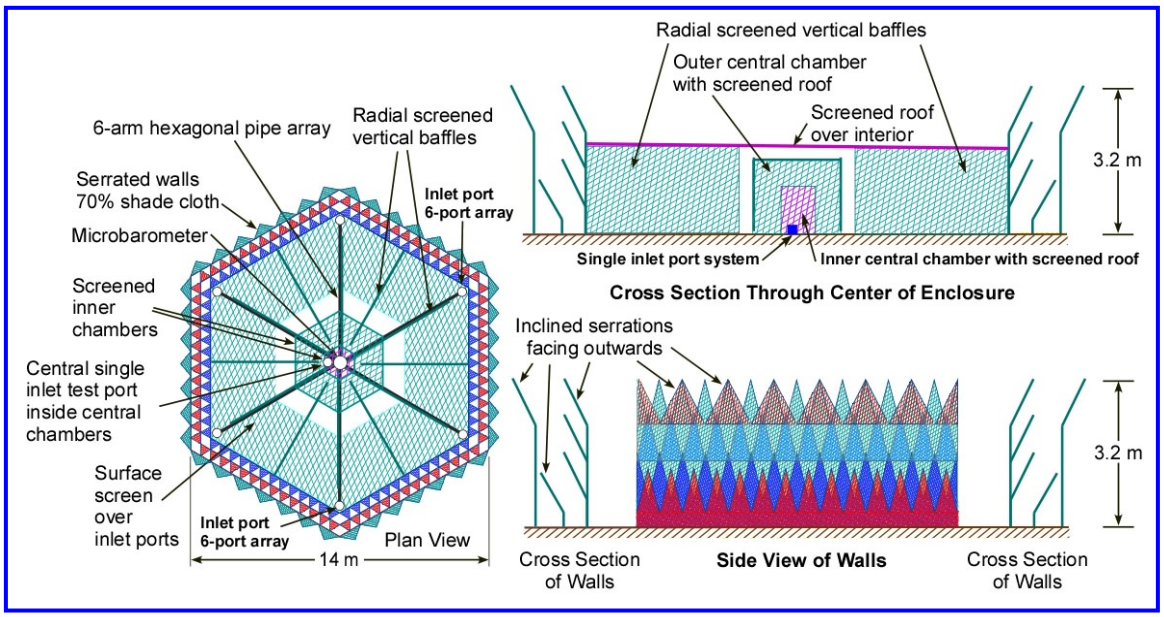


Figure 40. Schematic diagram illustrating Version 4B of the turbulence-reducing enclosure with 3.2-m high walls, radial baffles, interior screened chambers around a single-port system, a porous roof over the inner structure and a 6-port pipe array. Version 4B of the enclosure was tested over a six-week period in ambient winds in the range from 0.1 to 5.5 m/s. The results of these tests are presented in Figure 41. The overall performance of Version 4B of the enclosure is significantly better than the performance of Version 4A of the enclosure. This increase in performance can largely be attributed to the presence of the screened roof over the entire interior of the enclosure. Turbulence levels inside the enclosure were observed to decease dramatically after this roof was installed. As can be seen from the results shown in Figure 41, noise levels recorded inside the enclosure increase only very slowly as the ambient winds increase from 0.0 m/s to about 3.7 m/s

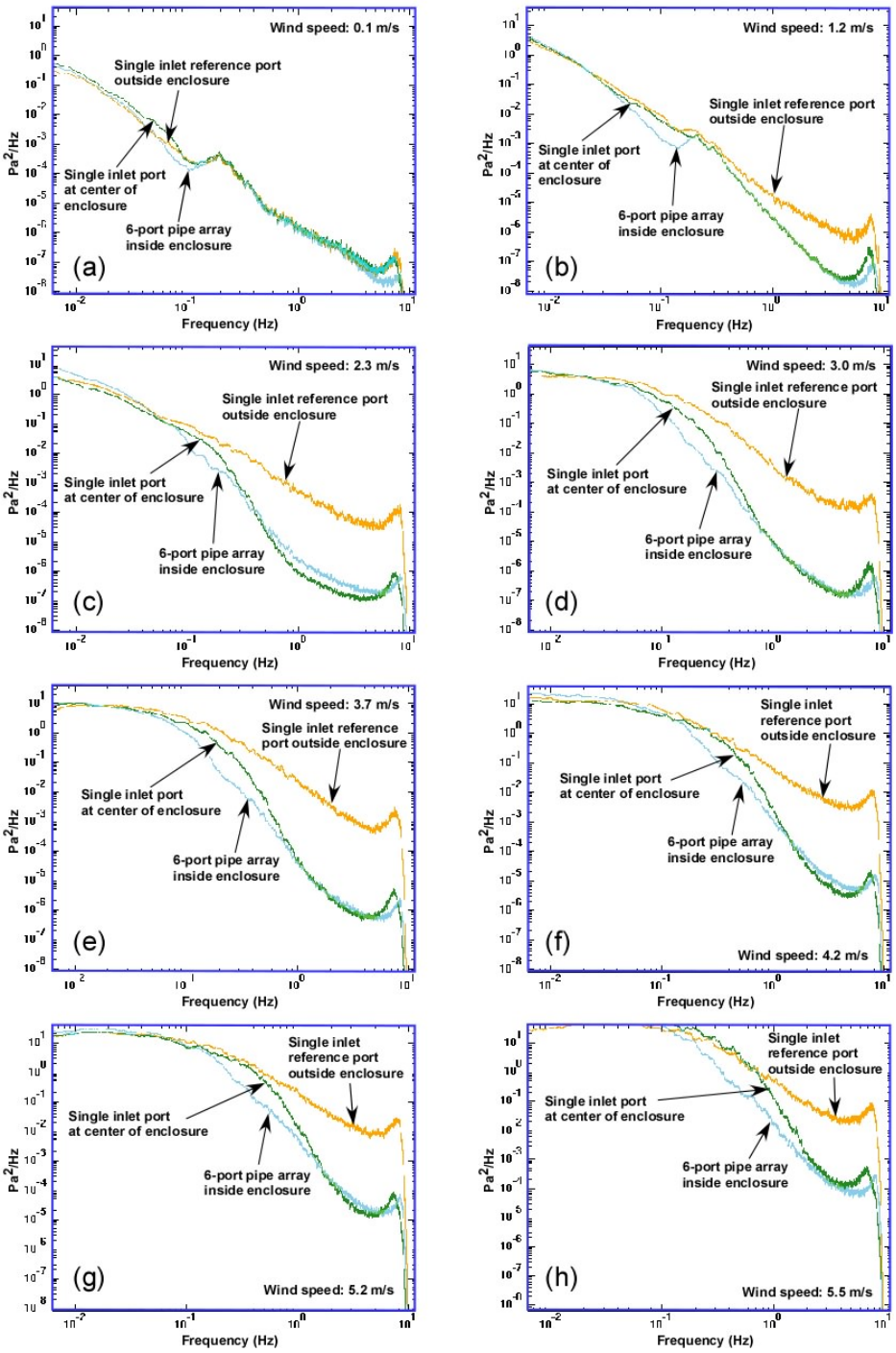


Figure 41. Comparison of power spectral density estimates of infrasonic data recorded with a 6-port pipe array system (light blue curve) and a single inlet port system (green curve) located inside Version 4B of the turbulence-reducing enclosure with power spectral density estimates of background noise data recorded simultaneously on a single inlet reference port located outside the enclosure (orange curve).

The performance of Version 4B of the enclosure with either a single inlet port system or a 6-port pipe array system is remarkably good in ambient winds of less than 3.7 m/s. Furthermore, the noise levels in this wind range are less than $5x10^{-5}$ $Pa^2$/Hz at 1.0 Hz, which is the essential design requirement for the upper bound on background noise at 1.0 Hz. Since the average maximum ambient winds during the daytime at IS07 over the year is about 3.5 m/s, Version 4B largely meets the requirements for a satisfactory wind-noise-reducing system at IS07 Warramunga. It is interesting to note that the performance of the single port system is generally better than the 6-port pipe array system at frequencies above 1.0 Hz in winds of around 2 m/s. The 6-port pipe array is, however, more effective than the single port system at lower frequencies. The performance of Version 4B is also very good in higher winds of up to about 5.2 m/s. However, as with all earlier versions of the enclosure, the performance starts to decrease rapidly as the ambient winds increase above 5.5 m/s. We believe that this can again be attributed to the interaction of the serrations on the top of the main walls of the enclosure with the higher wind levels at 3 m above the surface.

The results obtained to this point indicate that the inclined serrations on the top of the 3.2 m high walls on the outside of the enclosure may not be beneficial in higher winds. We therefore decided to make a major change in the design of the enclosure in order to avoid the direct interaction of the serrations with the ambient flow at higher levels. However, we recognize that we cannot simply remove these serrations from the upper edge of the structure since the incoming flow, which is partially blocked by the structure, will generate turbulence as the flow folds over the horizontal upper boundary of the structure.

In order to overcome this fundamental problem we have constructed Version 5 of the turbulence-reducing enclosure by:

a) Removing the portions of the outer serrated walls that extend above the 2.0 m high roof of the structure;

b) Introducing horizontal outward facing screened serrations in-line with the roof of the structure to limit the generation of turbulence in the flow over the upper edge of the enclosure. Since these serrations are horizontal, they do not interact with the incoming flow.

c) Introducing larger scale downward and outward facing screened serrations attached at the base of the serration to the upper edge of the outer wall of the structure. The purpose of these serrations is to degrade and break up incoming turbulent eddies before they reach the outer wall of the structure and also to further limit turbulent flow over the upper boundary of the structure.

d) Extending the main screened roof over the structure to cover the area between the two outside concentric walls, thus creating a fully closed enclosure. This should enhance the performance of the 6-port pipe array inside the structure.

A schematic illustration of Version 5 of the turbulence-reducing enclosure is given in Figure 42.

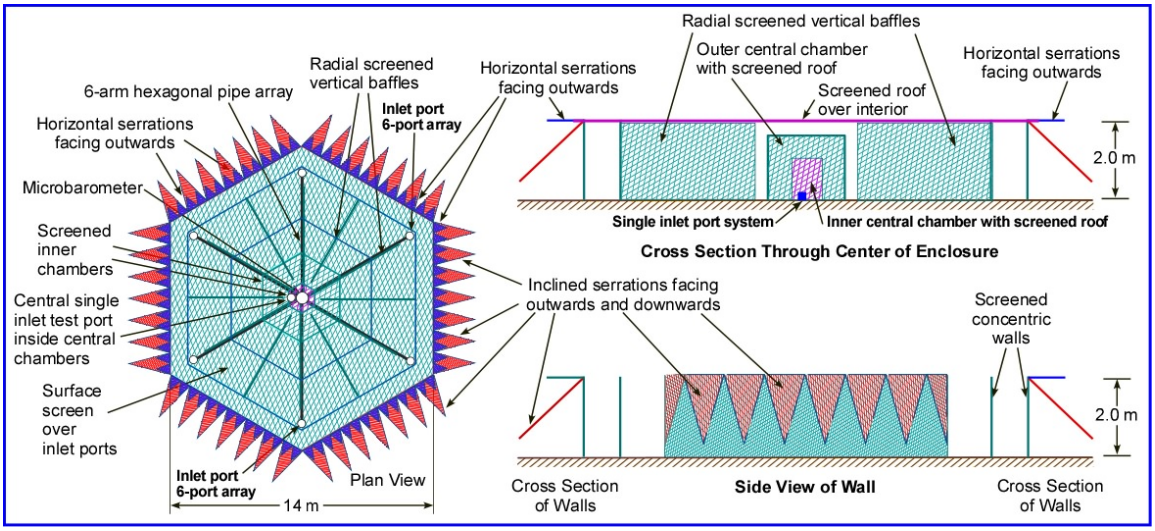


Figure 42. Schematic diagram illustrating Version 5 of the turbulence-reducing enclosure. All higher serrations on the outer walls have been replaced by (a) horizontal outward facing serrations and (b) larger scale outward facing and downward inclined serrations attached to the upper edge of the outer wall.

Version 5 of the wind-noise-reducing system has been tested in the relatively high-wind semi-desert environment at IS07 Warramunga in ambient winds ranging from 0.0 m/s to 6.0 m/s. A survey of the wind noise-reducing performance of this simplified, but highly effective, lower profile turbulence-reducing enclosure is presented in Figure 43.

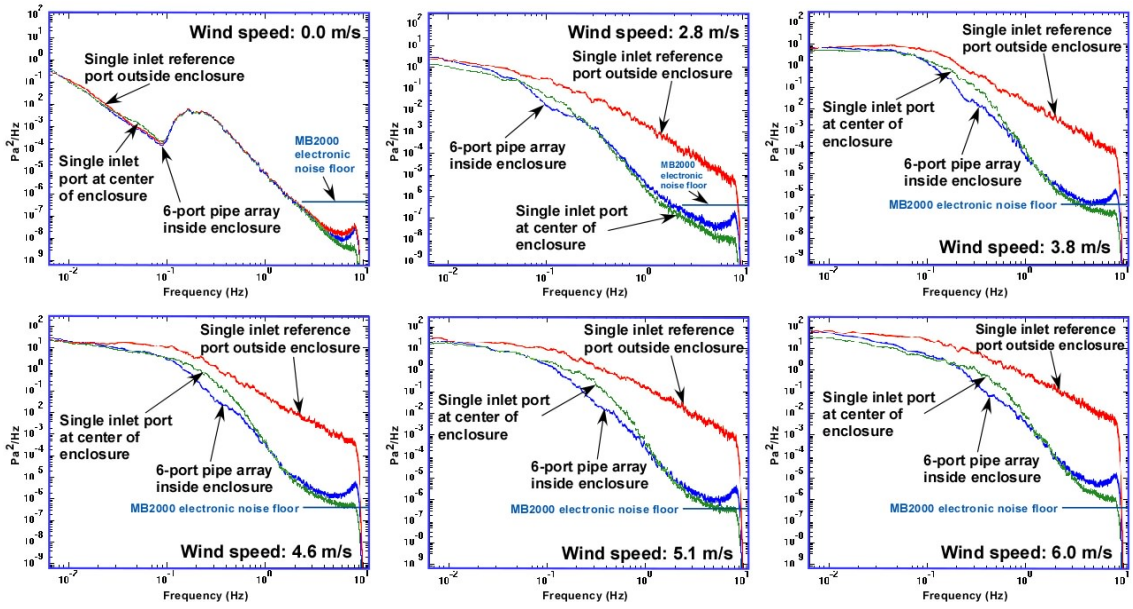


Figure 43. Comparison of power spectral density estimates of infrasonic data recorded with a 6-port pipe array system (light blue curve) and a single inlet port system (green curve) located inside Version 5 of the turbulence reducing enclosure with power spectral density estimates of background noise data recorded simultaneously on a single inlet reference port located outside the enclosure (red curve).

A comparison of the results presented in Figure 43 for Version 5 of the enclosure with the results presented in Figure 41 for Version 4B of the enclosure for background noise levels recorded in the same ambient wind speeds shows that Version 5 of the noise-reducing system has significantly better noise-reducing characteristics than Version 4B. We note that background noise levels recorded inside Version 5 of the enclosure at high frequencies are now at or below the electronic noise floor of the standard MB2000 microbarometer in winds of up to 3.8 m/s in the case of both the single inlet port system and the enclosed 6-port pipe array. The performance of the single inlet port system located inside the inner chambers near the center of the enclosure is almost always better than the performance of the enclosed 6-port pipe array at frequencies above 1 Hz. It is interesting to note as well that noise levels recorded on the single inlet port system at high frequencies are equal to or less than the electronic noise floor of a MB2000 microbarometer for ambient winds of up to at least 5.1 m/s. As in the case of Version 4B, the enclosed 6-port pipe array almost always performs better than the centrally located single port system at frequencies below 1.0 Hz. The single port system tends to have slightly better performance characteristics at 1.0 Hz than the 6-port array, but the 6-port pipe array is slightly more effective at 1.0 Hz in very high winds. Both systems exhibit very good noise-reduction characteristics at 1.0 Hz in ambient winds of up to about 5 m/s. In this case, wind-generated noise is attenuated by up to 4 orders of magnitude. The performance in higher winds is also significantly better than the performance found for Version 4B of the enclosure. Version 4B of the system was found to deteriorate rapidly when the ambient winds exceed about 5.5 m/s. Version 5 of the system is still very efficient at higher frequencies in ambient winds of 6.0 m/s, but performance at lower frequencies is starting to diminish at this point.

The high degree of noise reduction that has been achieved in the monitoring passband can be seen in the comparison of waveforms shown in Figure 44, which were recorded near noon in typical daytime wind conditions at IS07 Warramunga. The two upper traces in the diagram were recorded on the shielded single inlet port system and the 6-port pipe array located inside Version 5 of the enclosure. The bottom trace in this diagram was recorded simultaneously using a single inlet reference port system located outside the turbulence-reducing enclosure. It is clear from the results presented in Figure 44 that wind-generated noise in the primary monitoring passband has been dramatically reduced by Version 5 of the turbulence-reducing enclosure.

In view of the wavelengths involved and the porosity of the screens used in the construction of the turbulence-reducing enclosures, it can be anticipated that these structures will be virtually transparent to infrasonic signals with frequencies in the monitoring passband. The influence of Version 5 of the enclosure on the morphology of recorded infrasound signals has been examined in detail for a wide variety of signals at all frequencies of interest. In all cases, it was found that enclosures of this type have no observable influence on the waveform of infrasonic waves. This is illustrated in Figure 45 by a comparison of a typical signal generated by a small mining explosion recorded simultaneously both inside and outside the enclosure. The recorded signals are essentially the same with no indication of any phase shifts. We therefore conclude that the turbulence reducing enclosure is essentially transparent to infrasound and does not attenuate or distort infrasonic signals at frequencies in the monitoring passband.

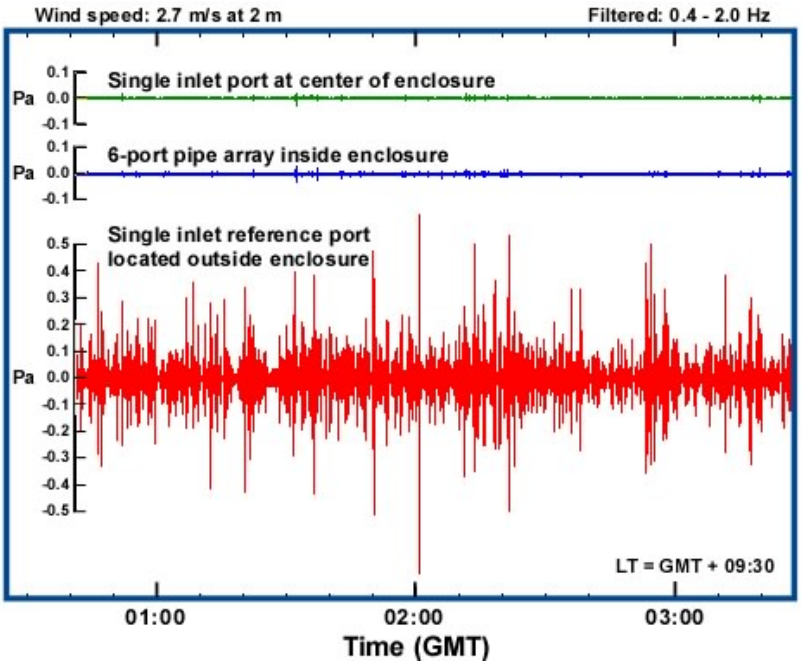


Figure 44. Comparison of background noise in the monitoring passband recorded on a single inlet port system and a 6-port pipe array system located inside Version 5 of the turbulence-reducing enclosure with background noise recorded simultaneously on a single inlet reference port located outside the enclosure. All traces have the same amplitude scale. The results clearly show that noise levels have been dramatically reduced by the turbulence-reducing enclosure.

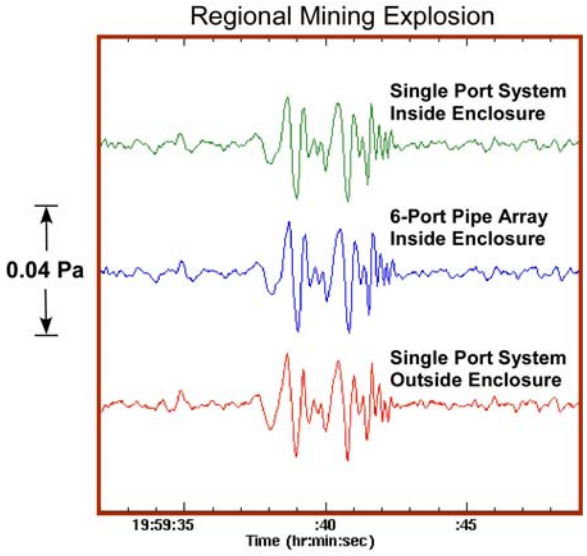


Figure 45. Comparison of infrasonic signals recorded simultaneously on a) single port systems located inside and outside the turbulence-reducing enclosure and b) a 6-port pipe array system located inside the enclosure. The signal was generated by a small mine explosion. This comparison shows that the closed turbulence-reducing enclosure does not attenuate or distort infrasonic signals

Version 5 of the wind-noise-reducing enclosure provides very effective wind-noise reduction in the primary monitoring passband. The performance of this relatively small enclosure with either a single port or a 6-port pipe array is significantly better than the performance of existing IMS pipe arrays. Pipe arrays have a number of disadvantages. They are relatively expensive to install and require a substantial area around each array element. In addition, pipe arrays are fairly complex acoustic systems with a number of unwanted resonances and the response of these systems is not always accurately known. They also distort and attenuate higher frequency signals, thus limiting the high frequency response of an infrasonic array. Wind-noise can be virtually eliminated at most infrasound stations by using Version 5 of the enclosure to enhance the performance of existing pipe arrays. We note as well that Version 5 can also be used in some cases as an effective stand-alone noise-reducing system that does not require a pipe array. Version 5 of the turbulence-reducing enclosure is 14 m in diameter. In contrast, existing pipe arrays at IMS infrasound stations are usually 18 m in diameter. The performance of the enclosures at longer periods is governed by the diameter of the structure. Turbulence-reducing enclosures that are 18-m in diameter will provide much better noise suppression at longer periods (and also at higher frequencies) than 14-m diameter enclosures.

### 4.3.2. Practical Considerations for the Construction of Turbulence-Reducing Enclosures

The following list provides some practical advice on the construction of turbulence-reducing enclosures for use at permanent infrasound monitoring stations:

a) The roof and all walls, including internal vertical baffles need to be constructed from porous screens. It is essential that the flow in and around the enclosure should not be completely blocked. The experimental structures described in this Report have been constructed using agricultural shade-cloth, a long-lasting robust product that is completely stable to ultraviolet radiation. All screens used in this project have a blockage factor between 50 and 70 %. The precise value of this blockage factor does not appear to be important, but it should probably not exceed 70%. Metal weatherproof screens (preferably industrial grade) may be used instead of shade-cloth at permanent installations. All screens should be as rigid as possible.

b) The screens should be supported on a rigid framework. This can be constructed at permanent stations using stainless-steel cables supported by galvanized fence posts with cement footings.

c) The supporting structure should be as rigid as possible. Torsional and lateral mechanical resonances need to be suppressed. These resonances can be removed by using appropriate stainless-steel guys at each corner post. Guys should also be used to secure the enclosure in high wind environments.

d) There should be no holes or gaps in the screening.

# 5. CONCLUSIONS

This investigation has been concerned primarily with the detection capability of stations in the global infrasound monitoring network for regional and distant nuclear explosions and the development of techniques that can be used to improve the performance of the global infrasound monitoring system.

The first part of this study is focused on problems associated with the decay of higher frequency signal components. It was found that observations of distant explosions may be limited to longer period components when propagation is restricted to a thermospheric waveguide. The essential conclusions from this study are:

a) Automatic routine signal processing for the monitoring of explosions should be carried out in passbands that span the complete frequency range from 0.01 Hz and 2.0 Hz, and

b) All infrasonic phases, including longer period thermospheric phases should be detected and used in location and discrimination algorithms.

The second part of this investigation is focused on problems associated with the low degree of signal correlation at higher frequencies between array elements in many existing infrasound monitoring arrays. It was found that the low degree of signal correlation between array elements in arrays with a small number of array elements may limit the reliable detection of regional and distant explosions at frequencies of 1.0 Hz and higher. These arrays need to be upgraded to 8- or 9-element arrays. The results of the signal correlation survey also show that the optimum passband for the detection of infrasound from atmospheric explosions with yields of less than a few kilotons spans the frequency range from about 0.4 to 1.2 Hz. It was also found that, even when an array has good side-lobe suppression characteristics, signal correlation between array elements in typical IMS arrays with 8 elements may be reduced substantially and the sensitivity of these arrays may exhibit significant azimuthal anisotropy at higher frequencies. A procedure was developed to calculate the predicted azimuthal distribution array-averaged correlation coefficient of arbitrary arrays with any number of array elements. This distribution provides a unique measure of the correlation properties of an array. This procedure was then used to design optimal infrasonic array configurations for monitoring regional and distant nuclear explosions. It was found that an optimal 8-element array for explosion monitoring is provided by an array configuration in the form of a 0.25-km aperture triangular sub-array located at the center of a 1.0 km aperture pentagon array. An optimal 9-element array is provided by a configuration in the form of a 0.30-km aperture centered triangle sub-array surrounded by a 1-km aperture pentagon array.

The third part of this investigation is focused on an attempt to completely resolve the infrasonic wind-generated background noise problem. It is clear that the elimination of wind noise at IMS infrasound monitoring stations would greatly enhance the monitoring performance and reliability of the global infrasound network. A large number of turbulence-reducing enclosures have been tested and the results are very encouraging. The latest version of the enclosure provides very effective (up to four orders of

magnitude) wind-noise reduction in the primary monitoring passband. The results described in Section 4.3 of this Report show that wind-noise can be virtually eliminated at most infrasound stations by using Version 5 of the enclosure to enhance the performance of existing pipe arrays. We note as well, however, that Version 5 can also be used at some infrasound monitoring stations as an effective stand-alone noise-reducing system that does not require a pipe array.

# 6. RECOMMENDATIONS

a) Automatic processing of data from the global infrasonic network should include:
   - A primary monitoring passband spanning the frequency range from 0.4 to 1.2 Hz, and
   - A long-period passband spanning the frequency range from about 0.04 to 0.1 Hz. Monitoring in this passband is required to ensure that signals can be detected from distant explosions when wave propagation is restricted to a thermospheric waveguide.

b) Signal correlation should be included explicitly in the design of infrasonic monitoring arrays.

c) New and upgraded infrasound arrays in the global monitoring network should be configured either in the form of a 0.25-km aperture triangle sub-array at the center of a 1-km aperture pentagon array or a 0.30-km aperture centered triangle array surrounded by a 1.0 km aperture pentagon array.

d) Large aperture arrays in the IMS infrasound network with a small number of array elements should be upgraded to one of the optimized pentagon arrays noted in (c).

e) The wind-noise-reducing techniques described in this Report should be implemented at all IMS stations with wind-noise problems. In order to effectively eliminate wind noise in the primary monitoring passband, we recommend that turbulence-reducing enclosures should be used in conjunction with 18-m diameter pipe arrays.

## REFERENCES


Alcoverro, B. (1998). Acoustic filters design and experimental results. Proceedings Workshop on Infrasound, DASE, Commissariat à l'Energie, Bruyères-le-Châtel, France, July 21-24

Alcoverro, B. and A. Le Pichon (2004). Design and optimization of a noise reduction system for infrasonic measurements using elements with low acoustic impedance, *J. Acoust. Soc. Am.* 117, 1717-1727.

Armstrong, W. T. (1998). Comparison of infrasound correlation over differing array baselines, *Proceedings of the 20th Annual Seismic Research Symposium*, Santa Fe, New Mexico, 543-554.

Bass, H. E. and F. D. Shields (2004). The use of arrays of electronic sensors to separate infrasound from wind noise, *Proceedings of the 26th Seismic Research Review*, Orlando, Florida, 601-607.

Bedard, Jr., A. J., B. W. Bartram, A. N. Keane, D. C. Welsh and R. T. Nishiyama (2004). The infrasound Network (ISNET): Background, design details, and display capability as an 88D adjunct tornado detection tool, *Proceedings of the 22nd Conf. On Severe Local Storms*, Hyannis, MA, Amer. Meteor. Soc., Paper 1.1.

Blandford, R. R. (1997). Design of Infrasonic Arrays. Air Force Technical Applications Center Report, AFTAC-TR-97-013.

Blandford, R. R. (2000). Need for a small subarray at IMS infrasound stations – Implications of shuttle and S. Pacific nuclear signals, *Proceedings Infrasound Workshop*, Passau, Germany.

Blandford, R. R. (2004). Optimal infrasound array design for 1kt atmospheric explosions, *Proceedings Infrasound Technology Workshop*, Hobart, Australia.

Campus, P, D.R. Christie and D.J Brown (2005). Detection of infrasound from the eruption of Manam Volcano on Jan. 27, 2005**,** *Proceedings Infrasound Technology Workshop*, Papeete, Tahiti.

Christie, D.R. (1989). Long nonlinear waves in the lower atmosphere, *J. Atmos. Sci*., 46, 1462-1491.

Christie, D.R. (2002). Wind-noise-reducing pipe arrays for IMS infrasound stations in Antarctica. Report IMS-IM-2002-1, International Monitoring System Division, Comprehensive Nuclear-Test-Ban Treaty Organization, Vienna, Austria, 10 pp.

Christie, D.R. (2006). Wind noise reduction at infrasound monitoring stations, *Proceedings Infrasound Technology Workshop*, Fairbanks, Alaska.

Christie, D.R. (2007). Recent developments in infrasound monitoring technology: Application to CTBT verification, *CTBTO Spectrum*, Issue 10, August 2007

Christie, D.R., J.A. Vivas Veloso, P. Campus, M. Bell, T. Hoffmann, A. Langlois, P. Martysevich, E. Demirovic and J. Carvalho (2001). Detection of atmospheric nuclear explosions: the infrasound component of the International Monitoring System, *Kerntechnik*, 66, 98-101.

Christie, D. R., B. L. N. Kennett and C. Tarlowski (2005a). Detection of distant atmospheric explosions: Implications for the design of IMS infrasound array stations, *Proceedings Infrasound Technology Workshop*, Papeete, Tahiti.

Christie, D. R., B. L. N. Kennett and C. Tarlowski (2005b). Detection of regional and distant atmospheric explosions, *Proceedings of the 27th Seismic Research Review*, Rancho Mirage, California, 817-827.

Christie, D. R., B. L. N. Kennett and C. Tarlowski (2006). Detection of atmospheric explosions at IMS monitoring stations using infrasound techniques, *Proceedings of the 28th Seismic Research Review*, Orlando, Florida, 882-892.

Christie, D. R., B. L. N. Kennett and C. Tarlowski (2007). Advances in infrasound technology with application to nuclear explosion monitoring, *Proceedings of the 29th Monitoring Research Review*, Denver, Colorado, 825-835.

Gossard, E. E. (1969). The effect of bandwidth on the interpretation of the cross-spectra of wave recordings from spatially separated sites, *J. Geophys. Res., 74, 325.*

Gossard, E. E. and Sailors, D. B. (1970). Dispersion bandwidth deduced from coherency of wave recordings from spatially separated sites, *J. Geophys. Res.,* 75, 1324-1329.

Gossard, E. E. and Hooke, W. H. (1975). Waves in the Atmosphere. Elsevier, New York. Chapter 9, Section 65.

Hedlin, M. A. H. and J. Berger (2001). Evaluation of infrasonic wind reduction filters, *Proceedings of the 23rd Seismic Research Review*, Jackson Hole, Wyoming, 121-130.

Hedlin, M. A. H. and R. Raspet (2003). Infrasonic wind-noise reduction by barriers and spatial filters, *J. Acoust. Soc. Am.* 114, 1379-1386.

Hedlin, M.A. H., B. Alcoverro and G. D'Spain (2003). Evaluation of rosette infrasonic noise reducing spatial filters, *J. Acoust. Soc. Am.* 114, 1807-1820.

Kennett, B. L. N., D. J. Brown, M. Sambridge, and C. Tarlowski (2003). Signal parameter estimation for sparse arrays, *Bull. Seism. Soc. Am.*, 93, 1765-1772.

Mack. H. and E. A. Flinn (1971). Analysis of the spatial coherence of short-period acoustic-gravity waves in the atmosphere, *Geophys. J. R. Astr. Soc.*, 26, 255-269.

McCormack, D. (2002). Towards characterization of infrasound signals, *Proceedings Infrasound Technology Workshop*, De Bilt, The Netherlands

ReVelle, D. O. (1998). Infrasonic Noise Reduction Using Shelters/Windbreaks, *American Geophysical Union*, Paper: A01E-05 .

Shields, F. D. (2005). Low-frequency wind noise correlation in microphone arrays, J. Acoust. Soc. Am., 117, 3489-3496.

Talmadge, C. L., D. Shields and K. E. Gilbert (2001). Characterization and suppression of wind noise using a large-scale infrasound sensor array, *Proceedings Infrasound Technology Workshop*, Kailua-Kona, Hawaii.

Walker, K.T., M. Zumberge, J. Berger, M.A. Hedlin and P.M. Shearer (2007). An improved method of back azimuth determination with a multi-arm OFIS, *Proceedings of the 29th Monitoring Research Review*, Denver, Colorado, 894-904.

Zumberge, M.A., J. Berger, M.H. Hedlin, E. Husmann, S. Nooner, R. Hilt and R. Widmer-Schnidrig (2003). An optical fiber infrasound sensor: A new lower limit on atmospheric pressure noise between 1 and 10 Hz, *J. Acoust. Soc. Am.* 113, 2474-2479.

## List of Symbols, Abbreviations, and Acronyms

| | |
|---|---|
| CTBT | Comprehensive Nuclear-Test-Ban Treaty |
| CTBTO | Comprehensive Nuclear-Test-Ban Treaty Organization |
| IMS | International Monitoring System |